CONFIDENTIAL

CLASSIFICATION CANCELLED

NACA

RESEARCH MEMORANDUM

RESULTS OF PRELIMINARY FLIGHT INVESTIGATION OF AERODYNAMIC

CHARACTERISTICS OF THE NACA TWO-STAGE SUPERSONIC RESEARCH

MODEL RM-1 STABILIZED IN ROLL AT TRANSONIC AND

SUPERSONIC VELOCITIES

By

Marvin Pitkin, William N. Gardner, and Howard J. Curfman, Jr.

Langley Memorial Aeronautical Laboratory
Langley Field, Va.

NATIONAL ADVISORY COMMITTEE
FOR AERONAUTICS

WASHINGTON
March 19, 1947

CONFIDENTIAL

CONFIDENTIAL

NATIONAL ADVISORY COMMITTEE FOR AERONAUTICS

RESEARCH MEMORANDUM

RESULTS OF PRELIMINARY FLIGHT INVESTIGATION OF AERODYNAMIC

CHARACTERISTICS OF THE NACA TWO-STAGE SUPERSONIC RESEARCH

MODEL RM-1 STABILIZED IN ROLL AT TRANSONIC AND

SUPERSONIC VELOCITIES

By Marvin Pitkin, William N. Gardner, and Howard J. Curfman, Jr.

SUMMARY

The design of a two-stage, solid-fuel, rocket-propelled, general research pilotless aircraft (RM-1) suitable for investigating stability and control at supersonic velocities is discussed. The flight-test investigation conducted thus far is discussed and information is presented on zero-length launchers and operational flight-test techniques of two-stage rockets.

The flight-test program thus far is shown to have resulted in the design of a general research model capable of attaining velocities up to the velocity corresponding to a Mach number of 1.4. Suitable launching methods have been devised and successful radar tracking and internal radio-transmission of acceleration data, pressure data, and body motions have been accomplished.

Results of initial flight tests confirm the theoretical advantage of swept-back-wing plan forms. Use of wings and fins swept back 45° delayed the critical drag rise to a Mach number of approximately 0.9. Successful roll stabilization by means of a rate-displacement, flicker-type, all-electric automatic pilot was accomplished for Mach numbers up to approximately 1.0. Information concerning the over-all drag characteristics of the RM-1 model at subsonic, transonic, and supersonic velocities is presented and discussed.

The results of the tests show close agreement among three experimental methods of measuring transonic and supersonic velocities.

INTRODUCTION

In recent years, it has become evident that a critical and urgent need existed for increased research on aircraft at transonic and supersonic velocities. During World War II, the accelerated development of jet propulsion and rocket motors resulted in the creation of power plants capable of propelling airplanes and guided missiles at supersonic velocities provided the aerodynamic and operational requirements of such aircraft were known. It was recognized at this time that pilotless aircraft, hitherto utilized solely as military weapons, offered one of the few means of examining the actual flight characteristics of airplanes at very high speeds. Such aircraft could be built to fly at supersonic velocities without endangering human life, and it was believed that techniques could be devised to measure fundamental aerodynamic and operational flight data and to transmit these data to ground stations.

Because of the foregoing considerations, the Pilotless Aircraft Research Division of the Langley Memorial Aeronautical Laboratory was created in May 1945 for the purpose of obtaining fundamental aerodynamic and operational data at transonic and supersonic velocities by conducting research on pilotless aircraft in flight. In order to accomplish this purpose, engineering facilities were made available at Langley Field, Va., and a test station was set up on Wallops Island, Va.

The first of several research airplanes to be designed was the RM-1 configuration, a two-stage, rocket-propelled aircraft designed to investigate stability and control problems in transonic and supersonic flight. A flight-test program of broad general scope was then started. Parts of this flight-test program have been completed. The present paper is concerned with the results of flight tests made to develop successful launching and operational techniques and with the significance of the data obtained in tests of an RM-1 model stabilized in roll flying at velocities up to those corresponding to a Mach number of 1.4. A discussion is also presented of the overall design and development of the test models.

SYMBOLS

W   gross weight of missile at any given time during flight, pounds

M   mass, slugs (W/g)

g   acceleration of gravity, 32.2 feet per second per second

L   lift normal to longitudinal body axis of RM-1 model, pounds

T   thrust along longitudinal body axis of RM-1 model, pounds

D   drag along longitudinal body axis of RM-1 model, pounds

a_L absolute longitudinal acceleration referred to RM-1 body axis, feet per second per second

a_N absolute normal acceleration referred to RM-1 body axis, feet per second per second

γ flight-path angle, degrees

t   time, seconds

Δt time increment, seconds

ΔV velocity increment, feet per second

$\Delta \gamma$ flight-path-angle increment, degrees

ϵ launching angle, degrees

ϕ angle of bank, degrees

$\ddot{\phi}$ rolling acceleration, radians per second per second $\left(\dfrac{d^2\phi}{dt^2}\right)$

M   Mach number (V/c)

V   velocity, feet per second

c   sonic velocity, feet per second

p_1 static pressure in free airstream, pounds per square foot

p_3 total pressure behind a normal shock, pounds per square foot

H   total pressure in free stream, pounds per square foot

F   maximum frontal area of RM-1 model, square feet

S   combined exposed area of wings and tail of RM-1 model, square feet

p   static pressure at altitude, pounds per square foot

k ratio of specific heat at constant pressure to specific heat
          at constant volume

C_D drag coefficient

A aspect ratio based on exposed area and span

Λ angle of sweepback, degrees

I_x moment of inertia, slug-feet^2

ANALYSIS OF PROBLEM

The purpose of the present investigation was to design and
place into operation a general research aircraft that could be used
to investigate stability and control problems in transonic and super-
sonic flight.

Preliminary analyses indicated that the problems of lateral
control and stabilization of high-speed aircraft were likely to be
most pressing because of the low rolling inertias and low rotary
aerodynamic damping characteristics of these designs. Consequently,
it was decided to attack these problems first.

The over-all plan involved three basic stages. First, the
model had to be designed to attain as high a speed as was practi-
cable with existent facilities and knowledge. Second, a preliminary
flight-test program was necessary to solve any operational diffi-
culties and to establish correct launching techniques. These tests
involved use of noninstrumented, or dummy, models. After these two
stages of development were accomplished, it was planned to equip
the models with instrumentation of various types capable of measuring
stability and control phenomena. This stage, in particular, required
the development and flight testing of an adequate telemetering system.
Once this aim was accomplished, it was felt that the RM-1 design would
be ready for research tests of various types of automatic pilot and
control.

DESIGN FOR SUPERSONIC VELOCITIES

An adequate propulsive system, low aerodynamic drag, and strict
weight control are the determining factors in the attainment of super-
sonic velocities. The problem confronting the designer was that of

designing an aircraft which would embody these factors and yet have adequate structural strength and space for instrumentation, and which would be easy to modify.

Propulsive System

Research tests require the development of high speeds only for the time interval necessary to measure the phenomenon under investigation. Consequently, a propulsive system insuring long flight range or duration was not necessary. This consideration eliminated the more involved types of jet-propulsion system (such as liquid-fuel rockets or ram-jet systems), and solid-fuel rockets were chosen as a propulsion source. In order to simplify instrument construction and operation, it was desired to keep launching and flight accelerations to relatively low values. Rockets of relatively low thrust and long firing times were therefore chosen in preference to high-thrust rockets of short firing times. The British 5-inch cordite rocket motor, rated at 1200 pounds thrust for 3.5 seconds, was considered to meet the power specifications and was chosen for use in the RM-1 model.

Preliminary calculations indicated that one rocket motor possessed insufficient power to carry the estimated payload and structure of the RM-1 model to supersonic velocities. An additional power boost was therefore required. In preference to using a catapult launching ramp which entailed a large expenditure of work and time, it was decided to design the RM-1 as a two-stage rocket. With such an arrangement, the test body of the RM-1 model would be attached to a booster tail rocket that would jettison itself after its fuel had been expended. Although the problems presented by a two-stage rocket system at first appeared formidable, it was felt that such an arrangement would ultimately prove superior to other methods of providing boost.

Aerodynamic and Structural Design

An over-all layout of the RM-1 configuration is presented as figure 1 and a photograph of the vehicle is shown as figure 2. The principles underlying the component design of this aircraft are discussed in the following sections.

Body design.- The results of the investigation reported in reference 1 show that increasing the fineness ratio of a body reduces its drag at supersonic velocities. Later results obtained in the Langley Flight Research Division indicate that fineness ratios

of the order of 12 to 15 percent may be optimum for low drag at
transonic velocities. A cylindrical body was therefore designed to
possess a fineness ratio as close to the optimum as possible and
yet be compatible with structural and installational requirements.
The diameter of the cylindrical body was restricted to 6 inches,
the minimum size required to house the sustaining rocket and yet
carry the estimated structural loads and internal apparatus. A
small conical nose was faired into the cylindrical part to form
a body of fineness ratio 22.5. This conical-nose section was chosen
after a study of the results of reference 2 which indicate that
this shape would probably be as good aerodynamically as more refined
shapes for use with bodies of large fineness ratio.

The RM-1 body was designed to consist of a series of magnesium
monocoque sections (see fig. 2), each section readily detachable from
the others and housing separate parts of the equipment. In addition
to the convenience of maintenance and installation, this feature
provides for rapid modification of body length. For tests of dummy
models, the sections in front of the wing were replaced by a solid
wooden body of identical shape and weight.

Wing and tail design.- Recent developments in Germany and the
United States (see references 3 and 4) have indicated the desirability
of utilizing swept-back plan forms to increase the critical Mach
number (delay the advent of compression shock) and hence to delay
the rise in drag and the loss of control effectiveness at transonic
and supersonic velocities. Although it was realized that sweepback
did not guarantee improved aerodynamic characteristics at speeds
exceeding that corresponding to the critical Mach number of the
swept-back sections, nevertheless its use appeared to offer the most
favorable approach to the problem of maintaining control throughout
the transonic and into the supersonic ranges of velocity. Wings and
fins of 45° sweepback, therefore, were incorporated into the RM-1
design. A sweepback angle of 45° was chosen because it was large
enough to indicate the influence of sweepback on aerodynamic character-
istics but small enough not to introduce any serious structural or
aerodynamic problems. Because of its high critical Mach number the
NACA 65-010 airfoil section was incorporated into the wing and fin
design.

In order to minimize the rolling moments created by airplanes
with swept-back plan forms when sideslipping at value of lift other
than zero, a cruciform design was adopted for the wings and tail fins
of the RM-1 model. With this arrangement the rolling moments created
by one set of swept-back wings are theoretically equal and opposite
to those created by the other set. Actually, unpublished test data
obtained in the Langley free-flight tunnel indicate that at moderate

and high angles of attack or sideslip, body-interference and partial-blanketing effects result in the creation of some rolling moments with sideslip. The wings and fins of the RM-1 model were constructed of laminated spruce stressed to take a 12g load.

Aileron-control design.- A plain-flap trailing-edge aileron control was chosen for the first tests of the RM-1 model. These ailerons are mounted on two diametrically opposite wings and are of 33 percent semispan and 10 percent chord. As shown in figure 3, the ailerons are equipped with a 20°-beveled trailing edge to provide aerodynamic balance at subsonic velocities and are completely mass-balanced to avoid flutter. They are hinged on a pin which is internally spring-loaded to provide for easy removal and installation. Stops are provided to limit the aileron travel to $\pm 10°$. The ailerons are constructed of cast magnesium to reduce their inertia and are mass-balanced by a strip of dense metal alloy which is attached to the leading edge of the control.

Booster-tail design.- A study of launching techniques indicated that the primary problem involved in the design of a second-stage or booster rocket is that of keeping the booster rocket carefully alined so that its line of thrust passes through the center of gravity of the airplane. If this alinement is not accomplished, the booster rocket will create large asymmetric moments that, at launching or low speeds at which the aerodynamic damping of the airplane is small, will result in violent maneuvering and eventual destruction of the airplane. It is also required that the booster separate positively but smoothly after firing to avoid jarring the main body and that these aims be accomplished with a minimum of additional weight. In addition, the rearward (destabilizing) movement of the center of gravity caused by booster attachment must be accounted for by addition of suitable stabilizing surfaces. These problems were solved as follows:

Cruciform triangular tail surfaces were attached to the rear end of the booster rocket to compensate for the loss in static stability caused by rearward movement of the center of gravity. The effectiveness of these surfaces was determined by the theory of reference 5 and checked by drop tests of $\frac{1}{10}$-scale dynamic models.

In order to avoid misalinement of the booster thrust axis, a special fixture was designed to attach to the front end of the booster rocket. This fixture (see fig. 4) was designed to utilize the nozzle of the sustaining rocket as an alinement jig. When assembled, the booster-fixture slide fits into the nozzle of the sustaining rocket and thereby prevents bending movements in any direction. The thrust of the booster rocket was transmitted to the lip of the sustaining-rocket nozzle so that no load was brought to bear on the internal plug. The booster fixture was also equipped with a compressed spring

which was designed to eject the booster from the sustaining nozzle after booster firing (in the event that the drag of the booster unit was insufficient). This spring was held in its compressed position by means of a friction-grip assembly tightened with two hollow bolts containing delay-ignition explosive caps. These caps were wired to the firing circuit and were set to release the friction grip after the missile was launched. The spring was released automatically after the booster thrust fell below 150 pounds.

Automatic-pilot design.- An all-electric, flicker-type automatic-pilot design consisting of one rate gyroscope and one displacement gyroscope, solenoid servomechanisms, and the trailing-edge aerodynamic control was designed to stabilize the RM-1 model in roll. This system was chosen because of its simplicity and because of its inherent quick-acting operation. A schematic layout of this system is shown in figure 5.

In operation, a deviation of the angle of bank and/or rolling velocity is detected by the gyroscopes which by means of a two-segment commutator, relay the proper electrical signal to the solenoid servomechanisms mounted in each wing. Energization of the servomechanisms causes an abrupt deflection of the aerodynamic controls.

The commercial rate gyroscope used in the RM-1 tests is equipped with stops which limit its action to angles of bank within $\pm 14^\circ$. At angles of bank greater than these limits, control signals are determined solely by action of the displacement gyroscope (right bank resulting in left aileron; left bank resulting in right aileron). Within the rate limits, however, the rate gyroscope primarily determines the time of signal reversal, being so arranged as to cause the control motion to lead the body motion. (Control reversal is accomplished prior to reversal of the angle of bank.)

Because it was realized that the time lag between the time of signal reversal and the time of full-control application would be the determining factor of the amplitude of the angle-of-bank oscillations under automatic control, every attempt was made to reduce the mechanical and electrical lag in the automatic-pilot system. Particular emphasis was given to reducing the time lag in the servomechanisms. The lag in servomechanisms, after development, was of the order of 0.03 to 0.05 second - values defining the time interval between the time an electrical signal was introduced into the solenoid coils and the time the aileron controls reached full opposite deflection ($\pm 10^\circ$). The power characteristics of the servomechanisms are shown in figure 6.

APPARATUS AND INSTRUMENTATION

Launching Apparatus

The RM-1 test bodies were launched from a zero-length launching ramp, a sketch of which is shown as figure 7. The launching ramp consists of a box beam mounted on a T-shape base and hinged at the junction of the T. The free end of the beam is supported on a pin-ended strut which can be adjusted to raise or lower the end of the ramp and thus adjust the missile launching angle.

When mounted on the launching ramp, the RM-1 model is supported either by two support arms or by one support arm and a tail rest. If the model is to be fired with a booster rocket, both support arms are used; if fired without a booster, one support arm and the tail rest are used. The support arms are hinge-pinned to the ramp and are held in a retracted position by elastic shock cords. When a model is mounted on the ramp, a component of its weight holds the support arms erect. When the rocket is fired, the elastic cord causes the arms to retract into the ramp in order to clear the path of the airplane. A photograph of the RM-1 model mounted on the launching ramp is shown as figure 8.

Radar Equipment

A continuous-wave Doppler effect radar set, the AN/TPS-5 (see fig. 9), was used to obtain velocity-time records of the RM-1 model during the early part of its flight. This radar set is a ground installation that transmits continuous radar signals of known frequency and wave length along a cone-shape path of vertex angle of 7°. Reflected radar echoes from a moving body are received by antenna mounted near the transmitter and are merged with the transmitted signals. The resultant beat frequencies are a function of the body velocities and are recorded as a trace on a chronograph device. The flight velocities are then determined from the chronograph records.

Radio Telemeter

Instrumented models of the RM-1 model were internally equipped with a four-channel radio telemeter developed by the Instrument Research Division of the Langley Laboratory. A photograph of the radio-transmitter part of this device is shown as figure 10. In operation, the movement of one of the instrument commutators modulates the

frequency of a subcarrier which, in turn, modulates the amplitude
of a high-frequency radio carrier. At the ground receiving stations,
the radio carrier is detected with a wide-band receiver and the sub-
carriers are fed to a set of four discriminators each of which is
tuned to one of the center frequencies of the subcarrier. The output
of each discriminator is proportional to the deviation of the input
frequency from the center frequency and is recorded by a multiple-
element recording galvanometer.

Photographic Apparatus

Photographic installations were used throughout the tests of
the RM-1 model to observe launcher operation and general flight
behavior. These installations included Mitchell 35-millimeter
motion-picture cameras, Ciné-Kodak 16-millimeter cameras, and Army
K-24 aerial cameras in ground implacements. The K-24 cameras were
used primarily to record launcher operation and operated at approx-
imately 3 frames per second. The Mitchell and Ciné-Kodak cameras
operated at 125 and 64 frames per second, respectively.

REDUCTION OF DATA

Accuracy

The items telemetered in some of the tests reported herein
were angle of bank, normal acceleration, longitudinal acceleration,
and total pressures. Experience has shown that the total error
involved in the telemetering of quantities such as these is of
the order of 1 percent of the maximum scale readings. Consequently,
the telemetered items are believed accurate within the following limits:

Longitudinal acceleration . . . .   ±0.16g

Normal acceleration . . . .   ±0.10g

Total pressure . . . .   ±0.5 in. Hg

Angle of bank relative to gyroscope reference . . . . .   ±0.9 deg

Determination of Flight Path

The flight-path characteristics of the RM-1 model were
determined as follows:

If the assumption is made that the static stability of the
RM-1 model is very large, the aircraft will tend to aline
itself with the relative wind at all times and the forces acting
on it are those shown in figure 11(a). Resolution of these forces
along the longitudinal and normal body axes of the model yields
the relationships

$$\sum \text{Longitudinal forces} = Ma_L = T - D - W \sin \gamma \qquad (1)$$

$$\sum \text{Normal forces} = Ma_N = -W \cos \gamma + L \qquad (2)$$

Dividing equations (1) and (2) by the mass M gives the acceleration
equations

$$a_L = \frac{T - D}{M} - g \sin \gamma \qquad (3)$$

$$a_N = -g \cos \gamma + \frac{L}{M} \qquad (4)$$

The quantities $\frac{T - D}{M}$ of equation (3) and $\frac{L}{M}$ of equation (4)

represent the relative accelerations of the RM-1 model and can
be directly obtained from telemetered acceleration data. Solution
of equations (3) and (4) for the flight-path angle γ by direct
mathematical methods is difficult because γ is a function of the
accelerations a_L and a_N. Consequently, recourse was made to a

step-by-step integration as follows:

Values of $\frac{T - D}{M}$ and $\frac{L}{M}$ against time were obtained from

telemetered records and the total time scale was divided into a
series of time increments Δt in length. When the value of a
quantity at the start of a time increment is denoted by the subscript
n and the value at the end of an increment by n + 1 the following
iterant relationships can be set up:

$$a_{L(n+1)} = \left(\frac{T - D}{M}\right)_{(n+1)} - g \sin \gamma_{(n+1)} \qquad (5)$$

$$a_{N(n+1)} = -g \cos \gamma_{(n+1)} + \left(\frac{L}{M}\right)_{(n+1)} \qquad (6)$$

where

$$\gamma_{(n+1)} = \gamma_n + \Delta\gamma$$

$$\Delta\gamma = \frac{a_{N_n}\,\Delta t}{V_{L_n} + a_{L_n}\,\Delta t} = \frac{\Delta V_N}{V_{L_n} + \Delta V_L} = \frac{\Delta V_N}{V_{L(n+1)}} \tag{8}$$

A vectorial representation of equation (8) is shown as figure 11(b). In order to start the trajectory calculations, it is necessary to know only the launching conditions. At time $t = 0$, the flight-path angle is equal to the launching angle ϵ, and V_{L_n} and V_{N_n} are zero. These conditions are assumed to persist through the first time interval.

During the time interval between $t = 0$ and $t = \Delta t$, therefore,

$$a_L = \left(\frac{T - D}{M}\right)_{\Delta t} - g\sin\epsilon \tag{9}$$

$$a_N = -g\cos\epsilon + \left(\frac{L}{M}\right)_{\Delta t} \tag{10}$$

where $\left(\frac{T - D}{M}\right)_{\Delta t}$ and $\left(\frac{L}{M}\right)_{\Delta t}$ are values taken from the telemetered data and averaged over the period Δt.

From equations (9) and (10), values of a_L and a_N during the first time increment can be determined. By use of equation (8), $\Delta\gamma$ and hence γ at the end of the first time period can be determined. The value of γ obtained in this manner can then be introduced into equations (5) and (6) with new values of $\frac{T - D}{M}$ and $\frac{L}{M}$ and the flight-path changes occurring in the second time increment then determined. The procedure is repeated for as long as desired and yields the time histories of the flight-path angle and the body velocities. Integration of the velocity curves will produce altitude and range data.

Determination of Velocity

Velocity values were obtained from the Doppler radar records by a simple mathematical treatment involving the recorded frequencies and the wave length of the transmitted radar wave.

Velocity data were obtained from telemetered longitudinal acceleration data by the following procedure:

The variation of longitudinal acceleration in g units with time was determined from the flight records. These values were corrected

to absolute accelerations by subtracting the gravitational acceleration component $g \sin \gamma$, where the flight-path angle γ is positive in climbing flight. The absolute acceleration was then plotted against time and the curve was integrated to yield longitudinal velocity.

Total-pressure measurements were converted to Mach number by utilizing the following theoretical expression obtained from equations in reference 6.

$$\frac{p_3}{p_1} = \frac{(k + 1)^{(k+1)/(k-1)} M^{2k/(k-1)}}{2^{k/(k-1)} (2kM^2 - k + 1)^{1/(k-1)}}$$

This expression defines the ratio of the total pressure behind a normal shock wave p_3 to the static pressure in the free stream p_1 in terms of Mach number M. The total pressure p_3 was obtained directly from test data. The static pressure p_1 was obtained from standard atmosphere tables (reference 7) after the determination of the RM-1 trajectory by methods discussed previously in the present section. The ratio of specific heats k was chosen as 1.4 for all calculations.

The speed of sound c used to convert velocity to Mach number, was obtained from the relationship

$$c = \sqrt{k \, PT}$$

where the gas constant for air R was chosen as 1716, and T is the absolute temperature in °F at altitude.

Drag and Normal Force

The drag of the RM-1 model in pounds was obtained by multiplying the telemetered power-off longitudinal acceleration in g units by the weight of the missile. A similar procedure regarding normal acceleration was used to obtain normal force. The drag coefficient was calculated from the relationship $C_D = \dfrac{D/FP}{\frac{k}{2} M^2}$. (See reference 1.)

In certain cases, this coefficient was corrected to plan-form area by multiplying C_D by the ratio F/S, where S is the combined exposed areas of four wings and four tails.

Angle of Bank

The telemetered records were converted to angle of bank
directly by use of preflight calibration results.

RESULTS AND DISCUSSION

Launching Characteristics

Calculations.- In order to estimate the launching characteristics
of the model, its drag and thrust characteristics were estimated,
and the step-by-step system of calculation discussed in the preceding
section was utilized to calculate the flight-path characteristics.
The estimated drag curve used in the calculations is shown in figure 12
and is based on results presented in references 1 and 8. Figures 13
and 14 present the calculated zero-lift trajectories of the RM-1 model
launched at different angles, with and without booster, for
design gross weights of 110 pounds for the basic body and 65 pounds
for the booster stage. The calculated variation of maximum velocity
with launching angle is shown in figure 15.

The launching calculations indicated that the second-stage
rocket would increase the maximum velocity of the RM-1 model by
approximately 33 percent. (See fig. 15.) It was also indicated
that the variation of maximum velocity with launching angle would
be small although highest velocities would be encountered at lowest
angles because of relieving gravitational effects.

A launching angle of 60° was selected for the tests because
lower angles produced trajectories less suitable for radar tracking
and higher angles caused unnecessary reductions in maximum speed.

The calculations also showed the necessity for strict weight
control. Figure 16 presents the variation of maximum velocity with
overload weight for the RM-1 model launched at 60°. These data
show a sizable reduction in top speed with increase in overload
weight, the top speed decreasing approximately 100 feet per second
for each 20 pounds added to the main body.

Dummy flight tests.- The first RM-1 model to be fired was
a dummy body of 127 pounds gross weight equipped with a booster tail.
The launching apparatus functioned perfectly in this test as in all
others, and released the model without any noticeable disturbances.
A photograph of the model leaving the launching ramp is shown as
figure 17. Although the aircraft functioned well during the early

part of its flight, it did not reach its top speed because of failure of the booster-rejection apparatus to reject the booster tail. Sentry circuits thereupon prevented the sustaining rocket from firing and the entire assembly remained together throughout the flight.

Although the model launching did not accomplish its ultimate aim, the results of the first test demonstrated that a two-stage rocket could be launched simply and satisfactorily from a zero-length launcher and that the stability of the missile plus booster tail was adequate. In order to determine the stability of the basic body, a second dummy RM-1 model was fired without a booster tail. (See fig. 18.) Again launching was unmarred and the air-craft control-fixed flight was completely stable.

The failure of the booster-rejection unit to function properly was believed to have arisen from failure, prior to flight, to compress fully the rejecting spring. (See fig. 4.) Consequently, the booster thrust jammed the alinement cone into the sustaining rocket nozzle and thereby prevented rejection of the booster tail. A new booster-rejection unit was therefore designed (see fig. 19) which avoided this difficulty and, in addition, lessened the weight of the unit.

The third dummy fired consisted of the basic body with the revised booster tail. All apparatus functioned as desired - launching and booster separation were accomplished without mishap. Radar records obtained in this test are shown converted to velocity in figure 20. These data indicated that the maximum speed measured in the test was well into the supersonic range (M = approx. 1.4) and of the order of the values calculated by the step-by-step procedure.

It was noted from motion-picture records of the third flight that the sustaining rocket fired almost immediately after the booster unit had been rejected. This condition arose as a result of the increase in the booster-rocket burning time due to the low atmos-pheric temperatures prevalent at the time of the test. This phenom-enon, if accentuated further, could have led to an explosion of the sustaining rocket due to blocking of its nozzle. Additional calcu-lations were therefore made to determine the effect of increasing firing lag between the two rocket stages. These results indicated only a small decrease in maximum velocity for reasonable time lags. Consequently, the arming circuits were rearranged to provide a less hazardous (2-sec) firing lag in the next tests.

Lateral Stabilization and Control Flight Tests

The conclusion of the dummy tests provided a pilotless-aircraft arrangement that could be launched, flown, and tracked up to velocities corresponding to a Mach number of approximately 1.4. The aircraft was therefore equipped with apparatus suitable for a quantitative lateral-control investigation. For this phase of the flight investigation, the model was equipped with its flicker automatic pilot and the four-channel telemeter.

Flight of fourth model.- The fourth model having a gross weight of 124 pounds was launched equipped with telemeter and automatic pilot. Although the launching was successful, the airplane failed to reach supersonic velocities owing to ignition failure of the sustaining rocket after the booster had been rejected. The velocity-time data obtained in this flight from the radar data are given in figure 21. The radar records show that the maximum speed attained by the RM-1 model was approximately 700 feet per second.

Because of the low speeds obtained in the fourth flight, only the angle-of-bank telemeter records possessed quantitative significance. These data indicated that satisfactory bank stabilization of approximately $\pm 4^\circ$ amplitude was obtained throughout the entire flight.

Flight of fifth model.- The launching of the fifth model, a configuration identical in shape and equipment with that of the fourth, was completely successful. No difficulty was encountered in launching; the telemeter operated satisfactorily throughout the flight; and the model was tracked by radar over most of its initial flight path. Time histories of the longitudinal and normal acceleration and total pressure obtained from the telemetered data are given in figure 22.

Velocity measurement.- A comparison of velocity data as obtained from integration of the longitudinal acceleration data, total-pressure measurements, and radar records is given in figure 23. These data indicate good agreement between the three experimental techniques of velocity measurement. Particularly good agreement (within ± 2 percent) was obtained at the transonic and supersonic velocities after the ignition of the sustaining rocket at $t = 5.75$ seconds (approx.). At lower velocities and times than those corresponding to this value, discrepancies in velocity values were more evident.

The acceleration data are believed to give the most accurate velocity measurement at small flight times and hence at low speeds. Since errors are accumulative in an integration process, however,

the velocity error should increase with time. Based on the telemeter accuracy previously mentioned (0.16g), velocity errors from acceleration data were estimated to be of the order of ±20 feet per second at speeds below 700 feet per second and about ±50 feet per second at maximum speed.

Actually, it is believed that the accuracy of the acceleration results is much better than the foregoing estimates because of the close agreement of the acceleration data with the total-pressure data at high speeds, where the total-pressure process is believed to be more accurate. At the top velocity recorded in the flight, it is believed that the total-pressure measurements are accurate within ±20 feet per second; however at low subsonic velocities the total-pressure data can have inaccuracies of over ±100 feet per second based on the previously mentioned telemeter accuracy (±0.5 in. Hg). Because the telemeter pressure commutator must be constructed in such a manner that it will be capable of measuring the high impact pressures associated with transonic and supersonic velocities, it cannot be expected to measure accurately the relatively low impact pressures associated with low subsonic velocities. The low-speed part of the velocity curve obtained from impact pressure data has therefore been omitted from figure 23.

The radar method of measuring velocity is believed to be the most accurate of the three methods employed. It is believed that velocity can be reduced from the radar data within ±10 feet per second of the true velocity values. This error is based on the fact that the longitudinal axis of the model is not constantly in line with the radar beam. It should be observed, however, that this technique, like the acceleration method, registers ground speed rather than airspeed and hence may differ from total-pressure values depending on the winds encountered in flight. On the firing date, the winds at altitude were less than 15 feet per second; hence their effect upon the correlation of velocity techniques should be small. Although the radar data were in excellent agreement with those obtained from other methods after t = 5.75 seconds, the radar data read low at times preceding this value. The reason for the discrepancy is believed to be that the radar was reading the velocity of the booster tail during the coasting period. For a short period of time, the booster would remain behind and directly in line with the model. Because of limitations in radar recording equipment, it was possible to obtain radar data for only a short period of time. In order to obtain the most valuable data, the equipment was not put in operation until approximately 4.5 seconds after the model was launched. As indicated in figure 23, no radar data are available after approximately 7.5 seconds. After this time, the trackers were unable to keep the radar beam on the model.

Inasmuch as the acceleration data agreed closely with other data at transonic and supersonic velocities and since the acceleration data are believed to be the most accurate data available at subsonic velocities, these data were used to define the velocity characteristics of the fifth flight of the RM-1 model.

A comparison of the results in figure 23 with those in figure 20 shows that the maximum velocity of the RM-1 model in its fifth flight was somewhat smaller than recorded by the radar for the third flight. This difference in maximum velocity is believed to be largely due to an inequality in rocket thrust. The thrust of the booster and sustaining rockets of the fifth model is shown in figure 24. These data were obtained by adding the drag in coasting flight to the thrust curves in power-on flight and indicate that the sustaining rocket of the fifth model produced less than its rated thrust (1200 lb). Calculations indicate that if the sustaining rocket had produced the same thrust as the booster rocket, a maximum velocity in excess of that corresponding to a Mach number of 1.4 would have been obtained.

Drag data.- The over-all drag and drag coefficient (based on maximum body frontal area) of the RM-1 model in power-off flight are shown plotted against Mach number in figure 25.

The drag data for the RM-1 model show that the wing and tail surfaces experienced sharp drag increases in the Mach number region between 0.95 and 1.04. A more gradual increase in the drag coefficient occurred at Mach numbers in the vicinity of 0.90 to 0.95. This drag rise was probably caused by shock losses on the fuselage inasmuch as data from reference 1 indicate that a high-fineness-ratio fuselage reaches its critical speed in this region.

At supersonic velocities, the drag rose more gradually causing a near-linear decrease in the drag coefficient.

Drag results for the RM-1 model are in agreement with theoretical predictions and test data measured by other investigators. The critical speed range noted in the present tests is in good agreement with that obtained in wing-flow tests of a wing plan form similar to that of the RM-1 model but of higher aspect ratio. (See reference 8.) In addition, the theory of reference 3 indicates that the critical Mach number of a section increases as the cosine of the sweep angle. The critical Mach number of an airfoil section (NACA 65-210) similar except in camber to the test section is estimated from low-speed pressure measurements at M = 0.75. (See reference 9.) If the gain in critical speed varied as the cosine of the sweep angle, the test wing would have been expected to reach its critical speed at M = 1.06. Three-dimensional effects were apparently responsible for reducing the gain in critical Mach number predicted by two-dimensional theory to values measured in the tests.

A comparison of drag-coefficient data for the RM-1 model with similar data obtained in tests of a research model (the RM-2 aircraft) equipped with 45° swept-back wings by the flight techniques of reference 10 is shown in figure 26. All drag coefficients shown in this figure are based on total exposed wing and tail area to facilitate a more direct comparison.

The data presented in figure 26 show that the drag characteristics obtained in tests of the RM-1 model are in agreement with those measured for the RM-2 model. The aircraft reached their critical velocities in the same region and their drag coefficients are in fair quantitative agreement. The higher drag coefficients of the RM-2 model are ascribed to obvious aerodynamic differences in the

Normal-acceleration data. - The normal-acceleration data plotted in figure 22 show that the missile received a sharp incremental normal disturbance (about 2g) when the sustaining rocket started firing. After the sustaining rocket was fired, only small values of acceleration normal to the longitudinal axis were experienced, which indicated that the missile was flying at a lift coefficient close to its design zero lift coefficient.

Lateral flight data.- The flight history of the lateral behavior of the RM-1 model as obtained from telemeter records is presented chronologically in figures 27 to 30. The results presented in figure 27 show that the model received a slight rolling disturbance upon launching. Corrective control by ailerons was apparently applied as indicated by the reversal of the bank curve. At the 1-second mark, the data indicate that the model received a large rolling disturbance causing it to diverge rapidly in left bank until the 3.7-second mark, at which time the control stopped the divergence and damped the motion to small values in slightly over 1 second. The cause of the rolling-moment disturbance is uncertain. The increasing slope of the bank curve after the 1-second mark would appear to indicate that the control was inoperative for a short time. Thus, it is possible that the control was jammed for approximately 2 seconds. It is also noted, however, that the time at which the control reversed the rolling motion (3.7 sec) corresponds to the time at which the booster thrust began to diminish. It is possible, therefore, that the rolling disturbance was induced by power effects possibly through inflow effects in the neighborhood of the booster tail surfaces.

Figure 28 shows that after the ailerons regained control of the model motions, excellent roll stabilization was obtained up to Mach numbers of 0.95 to 1.0. The presence of an out-of-trim rolling moment on the model is indicated by the asymmetry of the rolling curve within

one-half cycle. Figure 31 shows an enlargement of the actual
telemeter trace at Mach numbers near 1.0. An approximate estimate
of the size of this out-of-trim moment and the aileron effectiveness
was made by double-differentiating the bank curve of figure 31 near
its peaks (where rolling velocity, hence aerodynamic damping moments,
are zero) and by assuming that the gross torque (control moment
± out-of-trim moment) was equal to the inertia resisting moment $I_X \ddot{\phi}$.
This procedure indicated that at Mach numbers just below 1.0, the
out-of-trim moment was approximately 20 foot-pounds as compared with
a control moment of approximately 25 foot-pounds.

After a Mach number of 1.0 was reached the RM-1 model diverged
rapidly in roll although evidence of restoring control action
persisted up to a Mach number of 1.1. At velocities higher than
that corresponding to this value of Mach number the model rolled
continuously to the right with no evidence of operative control.

The failure of the automatic-pilot system to stabilize the model
occurred in the velocity region at which the swept-back wing became
critical as indicated by the drag data. (See fig. 25.) In this
region, test data obtained by means of the wing-flow method (refer-
ence 11) show that trailing-edge controls mounted on swept-back
wings undergo some loss of effectiveness. It is probable, there-
fore, that the rolling moments created by the RM-1 ailerons were
reduced at transonic and supersonic velocities to values at least
below that necessary to overcome the out-of-trim moments. It is
also possible that a rise in aileron hinge moments occurred at the
critical velocity, which overloaded the servomechanisms and pre-
vented control application. Further tests are required, however,
to determine the quantitative nature of these phenomena.

The telemetered data show that the RM-1 model rolled con-
tinuously to the right at Mach numbers above 1.1 at a rate of
approximately 1 cycle per second. As the model passed its peak
velocity and entered its coasting period, evidence of restorative
control again became evident as a Mach number of 1.1 was reached.
(See fig. 29.) At a Mach number of 0.97, the control was sufficiently
effective to halt and reverse the rotation and good stabilization was
again achieved at subsonic velocities.

The subsonic rolling oscillation is shown in figure 30 and is
typical of the oscillation induced by a rate-displacement flicker-
type automatic pilot. If stops prevent the deflection of the rate
gyro (as was true for the tests) the displacement gyroscope governs
corrective control signal at large displacement angles. When the
angle of bank is reduced to smaller values, the rate gyroscope governs
signal reversal and a high-frequency, small-amplitude oscillation is
created within the angular range controlled by the rate gyroscope.

The data of figure 30 indicate that the RM-1 model tended to stabilize about a mean value of approximately 22° right bank. This value is believed to be in error because signal reversal is not possible with the automatic pilot employed at angles of bank greater than ±14° (the outer limits of the rate band) provided that the spin axis of the displacement gyroscope is in the plane of symmetry of the airplane. (See fig. 5.) It is probable, therefore, that the displacement gyroscope precessed during the accelerated part of the flight and caused a rotary shift of its reference position to the right.

The pertinent characteristics of the subsonic rolling oscillation have been summarized in figure 32 and show that both the amplitude and the period of the oscillations increased with increase in forward velocity. The amplitudes of the rolling oscillation during the coasting flight are larger than those at the same speeds in accelerated flight probably because of the greater initial rolling disturbance induced by the continuous right spiral at supersonic velocities. The tendency of the rolling oscillations to increase with velocity is due to the fact that the rolling velocities induced by a given control deflection also increase with speed. Consequently, for a given automatic-pilot time lag (time between detection of body deviation and time of control application) the amplitude and period will vary as a function of the rolling velocity and hence will increase with airspeed. It can be seen that in order to obtain supersonic roll stabilization of the order obtained at subsonic velocities it will be necessary either to decrease the time lag of the automatic pilot or to reduce by some means the rolling velocities.

CONCLUDING REMARKS

A basic research vehicle capable of attaining flight speeds up to those corresponding to a Mach number of 1.4 has been designed, developed, and put into operation. Zero-length launchers and various flight operational techniques have been devised which permit the successful operation of two-stage, rocket-powered, pilotless aircraft, and instrumentation has been developed which permits the transmission of data from a body moving at supersonic velocities.

Data obtained from initial flight tests confirm the theoretical advantage of swept-back wings. Drag values obtained at transonic and supersonic velocities were in general agreement with those measured by other flight techniques. Successful roll stabilization

by means of a rate-displacement flicker-type all-electric automatic
pilot was accomplished up to a Mach number of approximately 1.0.
Excellent agreement was reached among three methods of measuring
transonic and supersonic velocities.

Further tests are required to develop aerodynamic controls and
configurations suitable for operation at supersonic velocities and
to develop means of providing adequate stabilization within this
region.

Langley Memorial Aeronautical Laboratory,
        National Advisory Committee for Aeronautics,
                Langley Field, Va.

REFERENCES

1. Thompson, Jim Rogers, and Mathews, Charles W.: Total Drag of a
      Body of Fineness Ratio 12 and Its Stabilizing Tail Surfaces
      Measured During Free Fall at Transonic Speeds. NACA CB
      No. L6D08, 1946.

2. Ferri, Antonio: Supersonic-Tunnel Tests of Projectiles in
      Germany and Italy. NACA ACR No. L5H08, 1945.

3. Jones, Robert T.: Wing Plan Forms for High-Speed Flight. NACA
      TN No. 1033, 1946.

4. Busemann, A.: Aerodynamischer Auftrieb bei Uberschallgeschwin-
      digkeit. Luftfahrtforschung, Bd. 12, Nr. 6, Oct 3, 1935.
      pp. 210-220.

5. Jones, Robert T.: Properties of Low-Aspect-Ratio Pointed Wings
      at Speeds below and above the Speed of Sound. NACA TN
      No. 1032, 1946.

6. Taylor, G. I., and Maccoll, J. W.: The Mechanics of Compressible
      Fluids. Two-Dimensional Flow at Supersonic Speeds. Vol. III
      of Aerodynamic Theory, div. H, ch. IV, sec. 3, W. F. Durand,
      ed., Julius Springer (Berlin), 1935, p. 241.

7. Diehl, Walter S.: Standard Atmosphere - Tables and Data. NACA Rep.
      No. 218, 1925. Reprint 1940.

8. Zalovcik, John A., and Adams, Richard E.: Preliminary Tests at
      Transonic Speeds of a Model of a Constant-Chord Wing with a
      Sweepback of 45° and an NACA $65_{(112)}$-210, a = 1.0 Airfoil
      Section. NACA ACR No. L5J16a, 1945.

9. Heaslet, Max A. and Pardee, Otway O'M.: Critical Mach Numbers of
      Thin Airfoil Sections with Plain Flaps. NACA ACR No. 6A30, 1946.

10. Alexander, Sidney R., and Katz, Ellis: Drag Characteristics of
      Rectangular and Swept-Back NACA 65-009 Airfoils Having Aspect
      Ratios of 1.5 and 2.7 as Determined by Flight Tests at Super-
      sonic Speeds. NACA RM No. L6J16, 1946.

11. Daum, Fred L., and Sawyer, Richard H.: Tests at Transonic Speeds
      of the Effectiveness of a Swept-Back Trailing-Edge Flap on
      an Airfoil Having Parallel Flat Surfaces, Extreme Sweepback,
      and Low Aspect Ratio. NACA CB No. L5H01, 1945.

CONFIDENTIAL

Antenna and instrument pickoffs

Telemeter — Automatic pilot

C.G. rocket loaded

Cordite rocket motor (sustaining)

45°

6.0 Diam.

0   30.0   43.5   63.5   84.5   136.0

←——— 40.0 ———→

15.0

5.0 Diam.

Booster rocket motor,
ejector unit, and fins

	Wings	Fins
Span	26.00 in.	20.46 in.
Chord (min.)	10.00 in.	7.21 in.
Chord (max.)	14.14 in.	10.20 in.
Sweepback	45°	45°
Area (exposed)	565 sq in.	293 sq in.
Airfoil (min. chord)	NACA 65-010	NACA 65-010
Fuselage		
Length	136 in.	
Diameter	6 in.	
General		
Rocket motor:		
Weight (loaded)	67 lb	
Weight (empty)	40 lb	

CONFIDENTIAL

Figure 1.- Over-all design features of the
NACA supersonic control-
research model, RM-1.

Fig. 1

Figure 2.- Component design of RM-1 model.

Fig. 2

CONFIDENTIAL

CONFIDENTIAL

NACA 65-010

45°

14.14

10

10

3

$1\frac{1}{2}$

$4\frac{5}{16}$

A

A

A-A

4°

0.52

1.52

0.158

10°

Center line of model
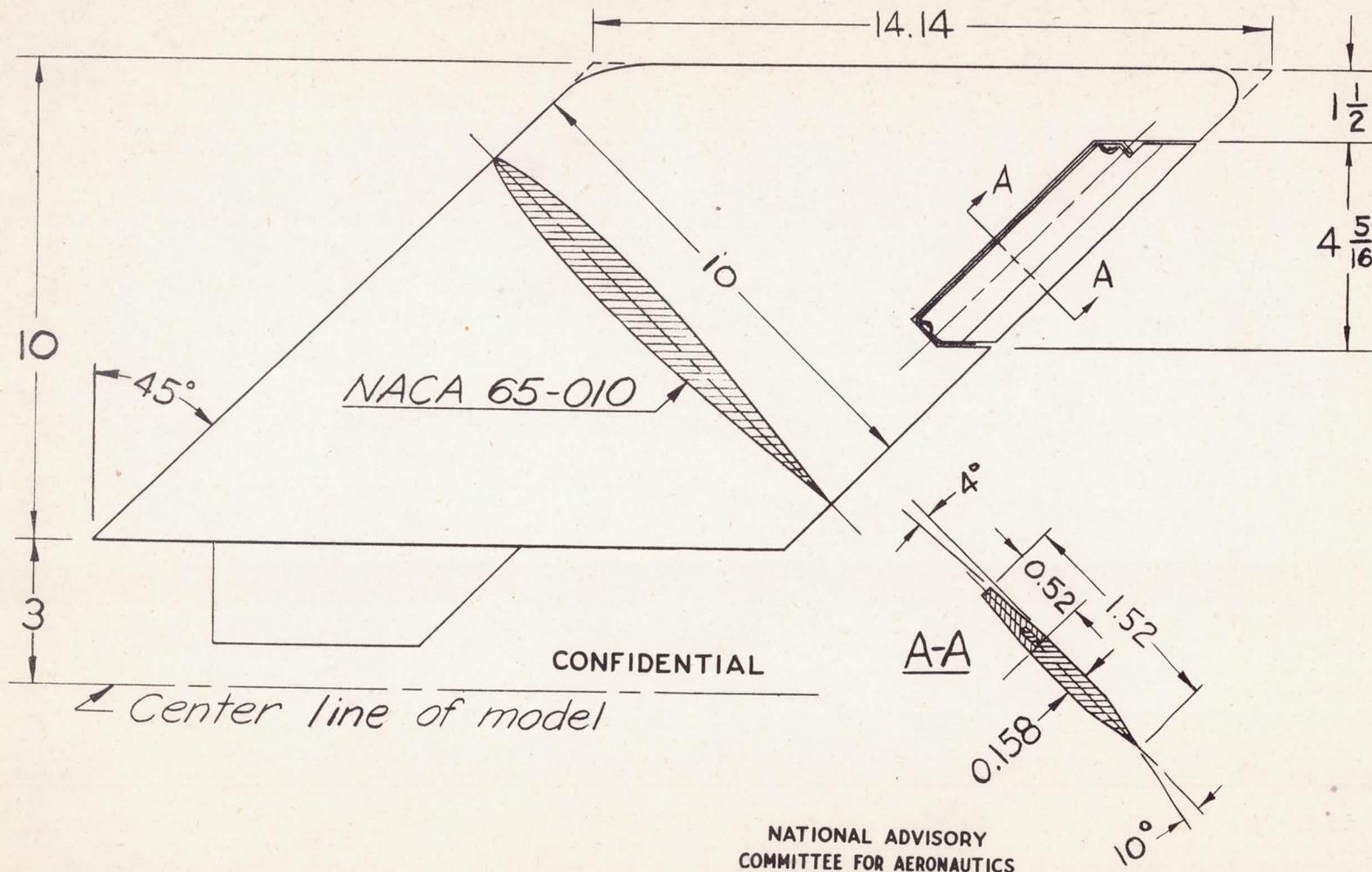
Figure 3.- Wing-aileron installation of the
RM-1 configuration.

Fig. 3
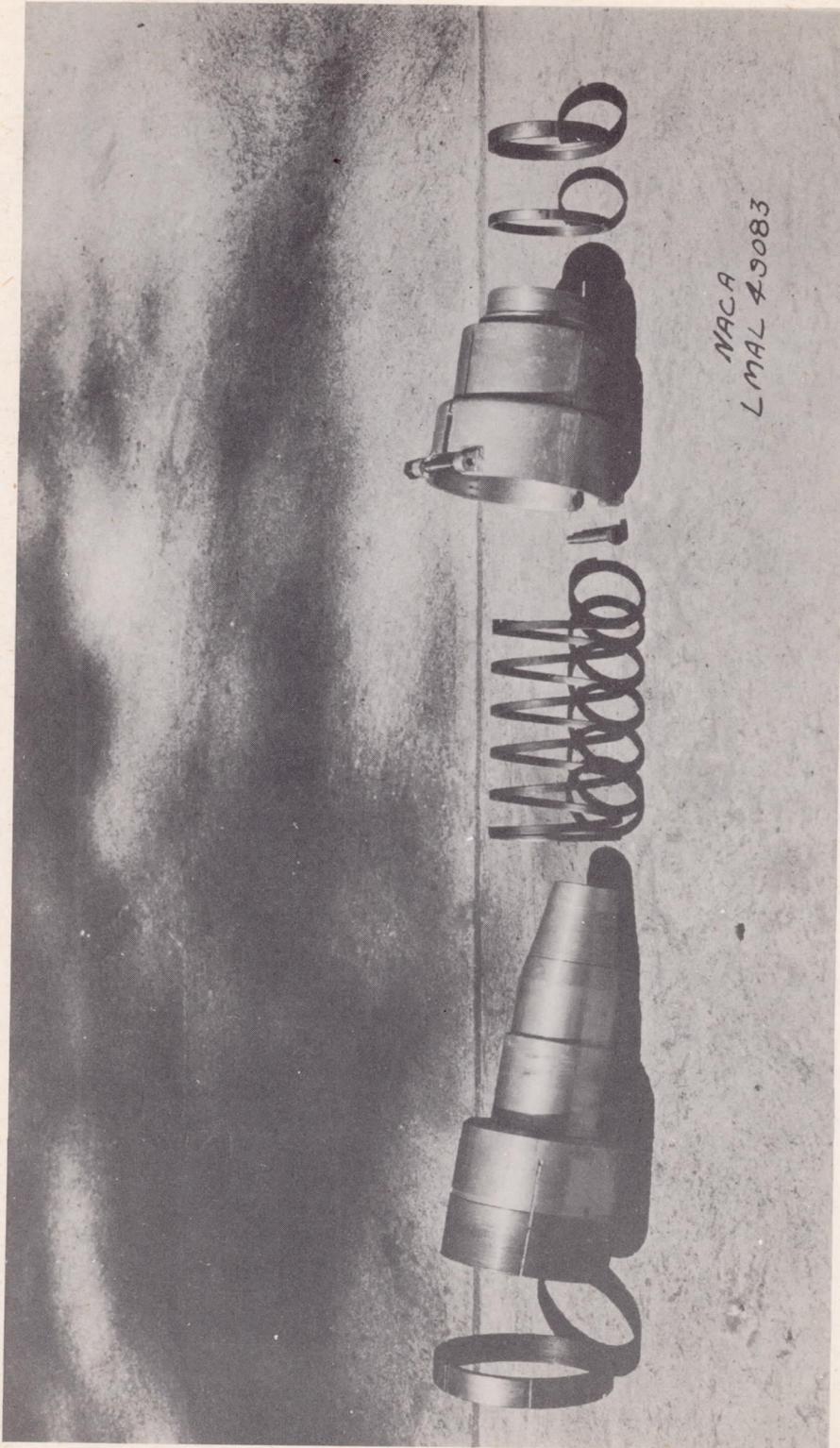
Figure 4.- Initial booster-rejection mechanism of RM-1 model.

CONFIDENTIAL

Rider arm
(attached to outer
gymbal of displace-
ment gyro)

Power

Comutator drum (attached to
mounting case of displacement gyro)

Right | Left

Signal | Signal

Relay

Displacement gyro axis

Rate gyro

Electromagnetic
servomechanism
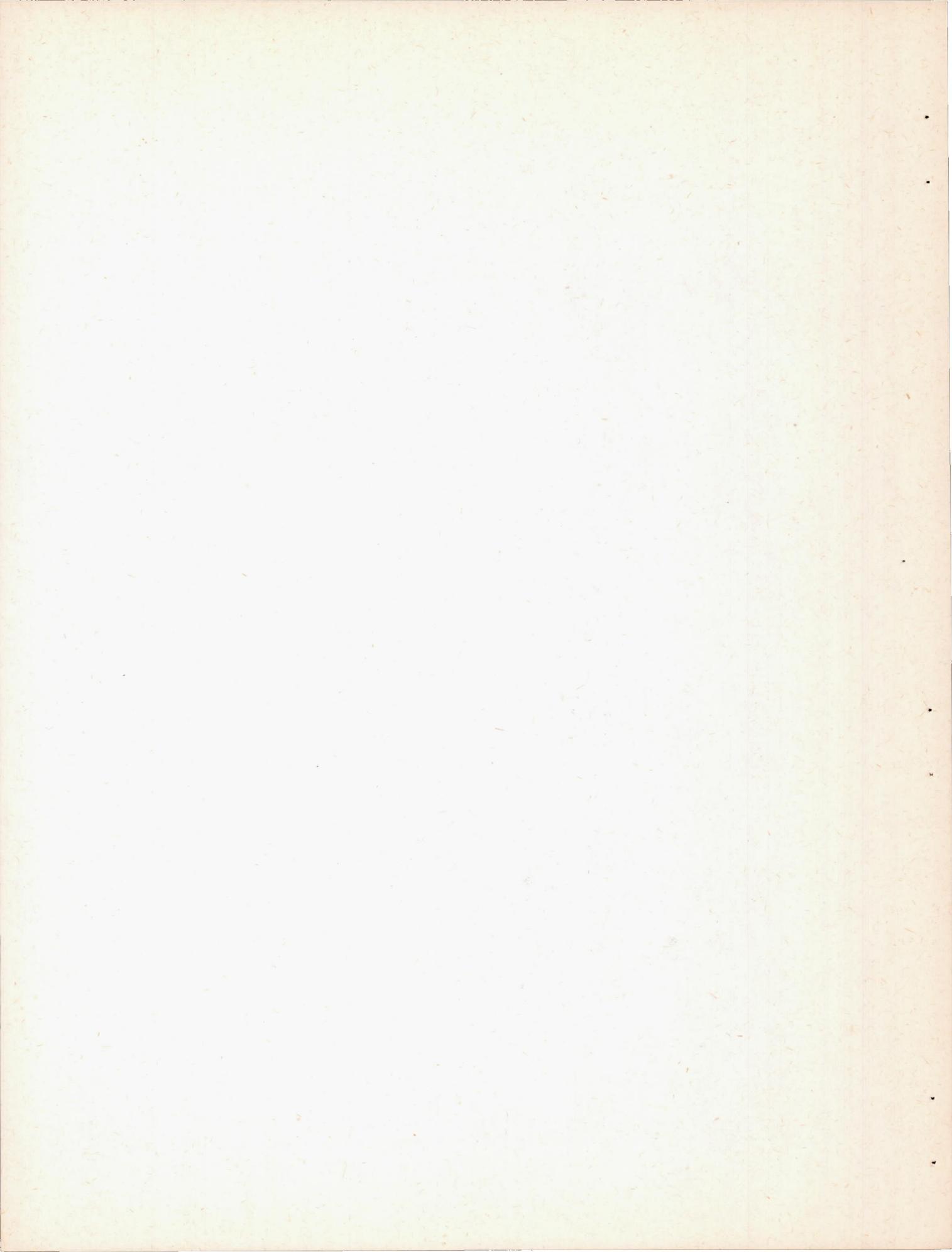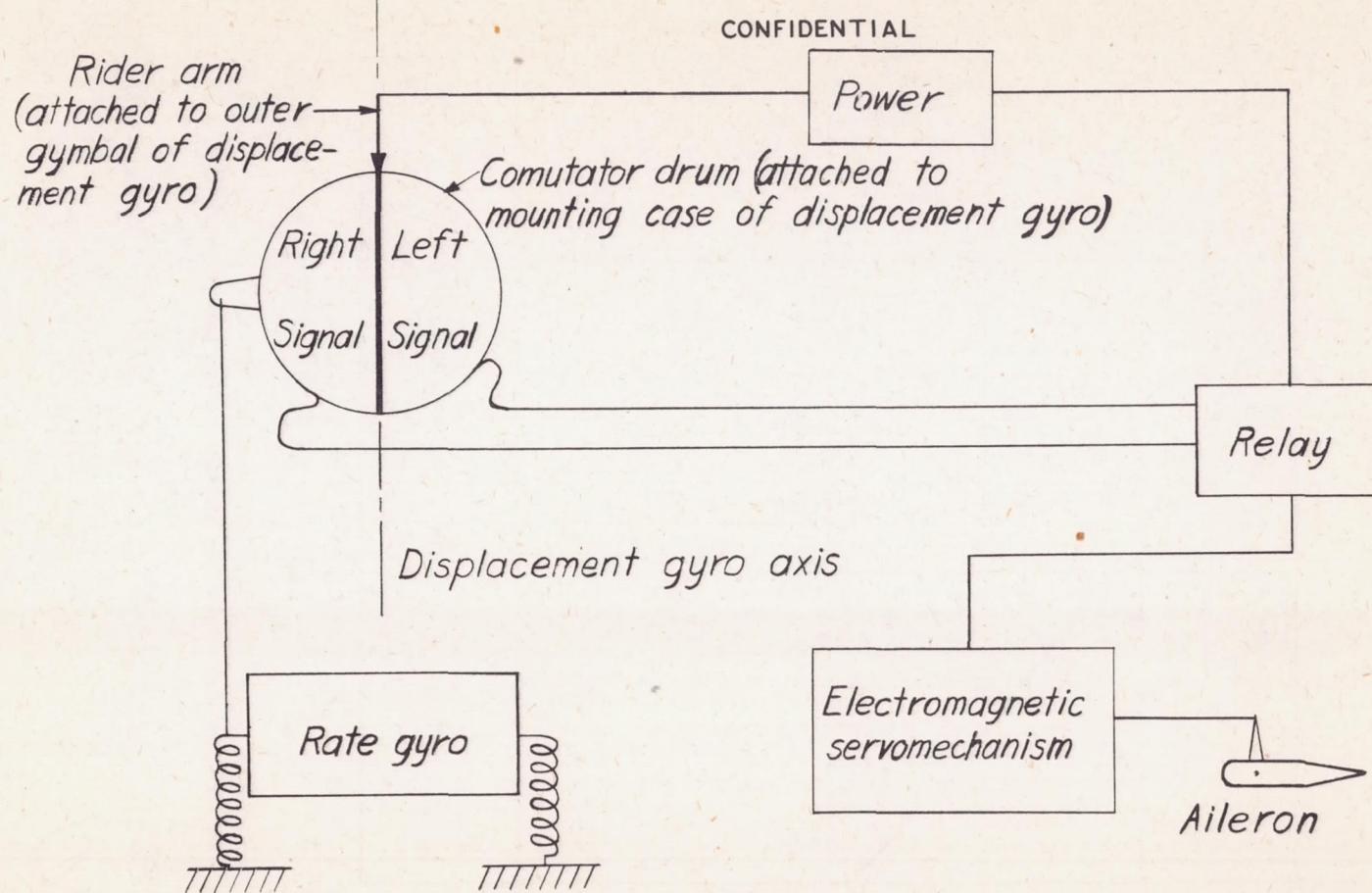
Aileron

CONFIDENTIAL

Figure 5. — Schematic diagram of RM-1 automatic pilot.

Fig. 5

Fig. 6   NACA RM No. L6J23
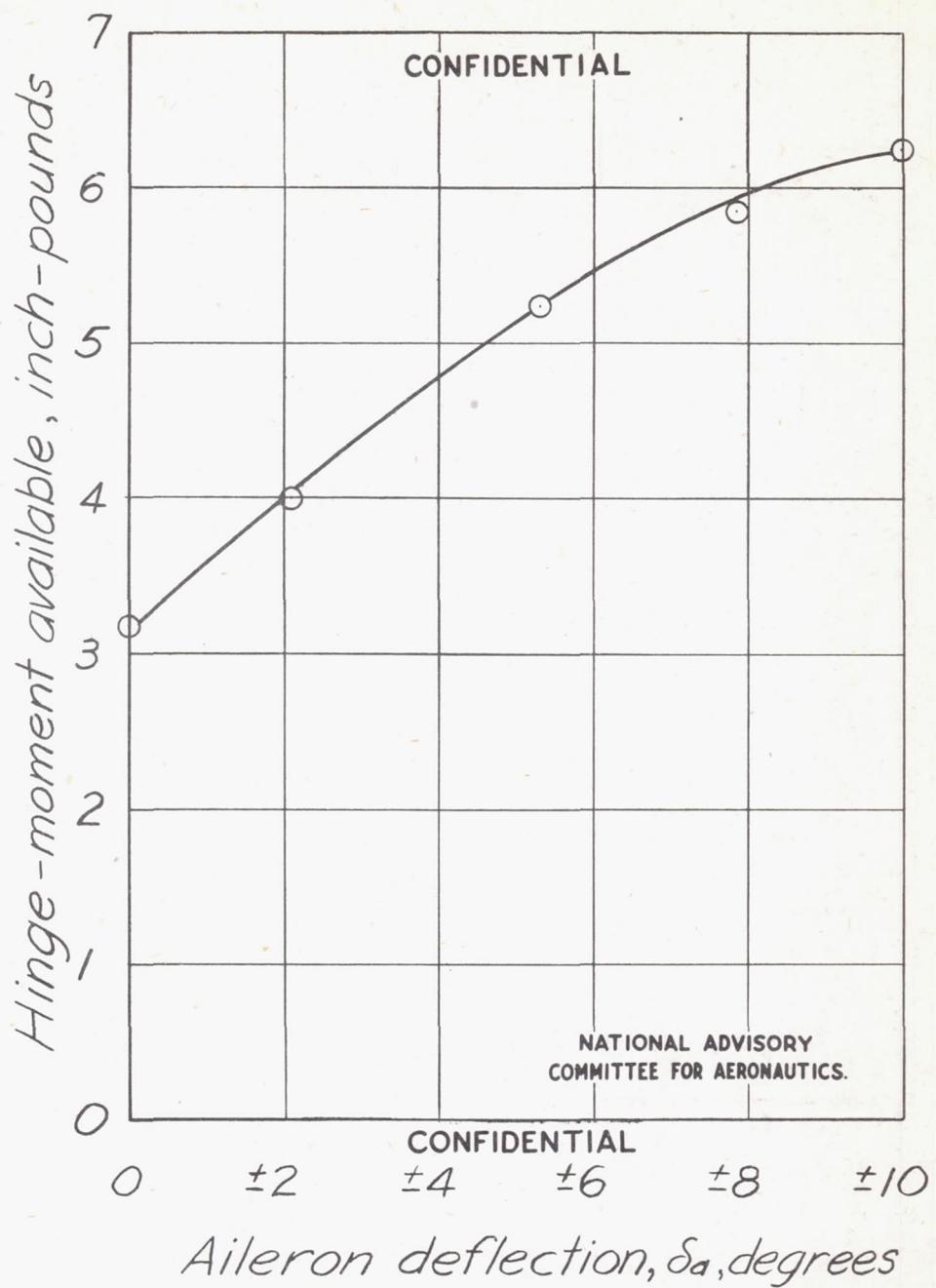
Figure 6.- Servomechanism characteristics of RM-1 model for one aileron.

CONFIDENTIAL

RM-1 in launching position

Position of
support arms
after launching

Tail support not used
when model is launched
with booster rocket
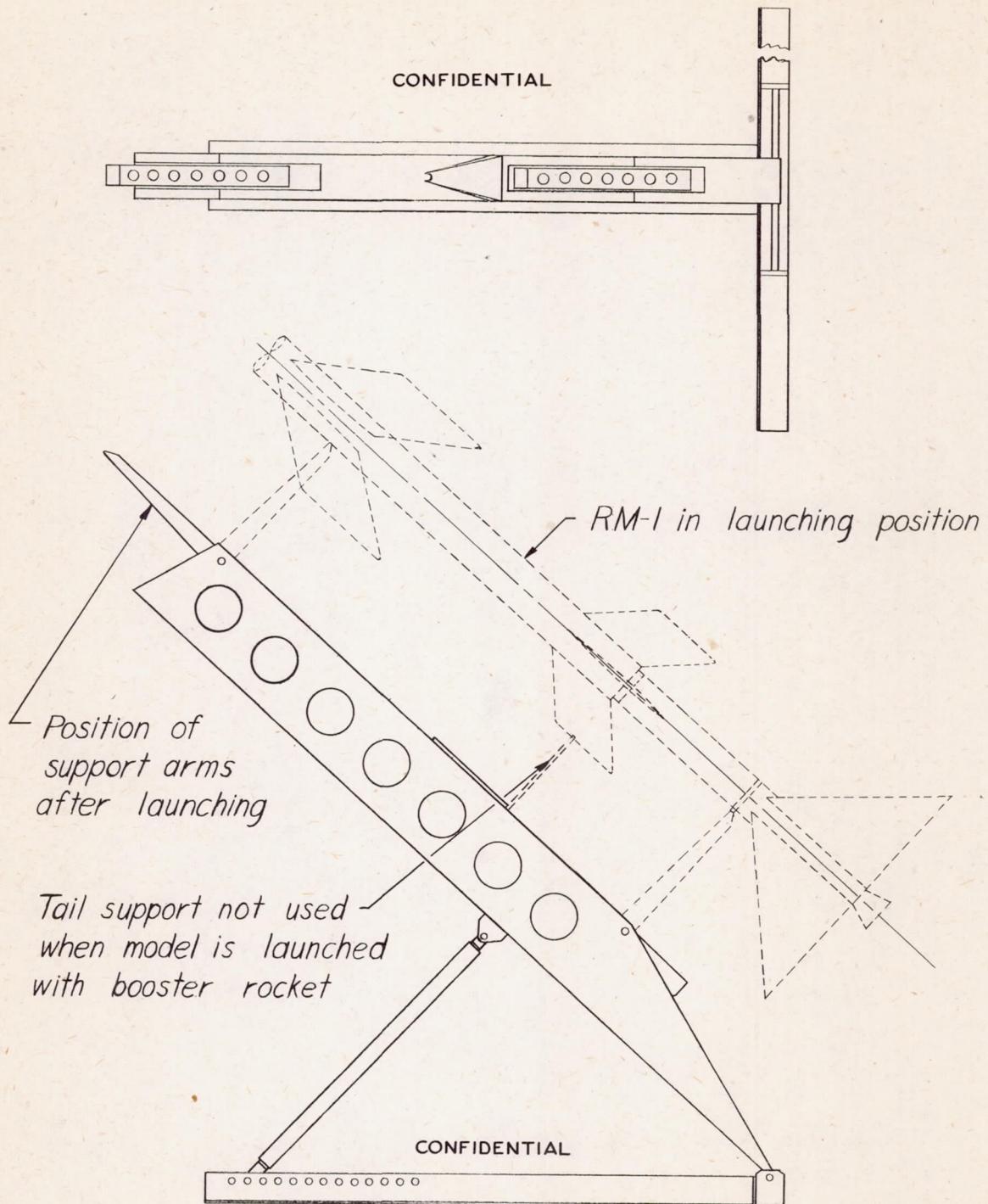
CONFIDENTIAL

Scale
0   10"

Figure 7. — RM-1 launching rack.
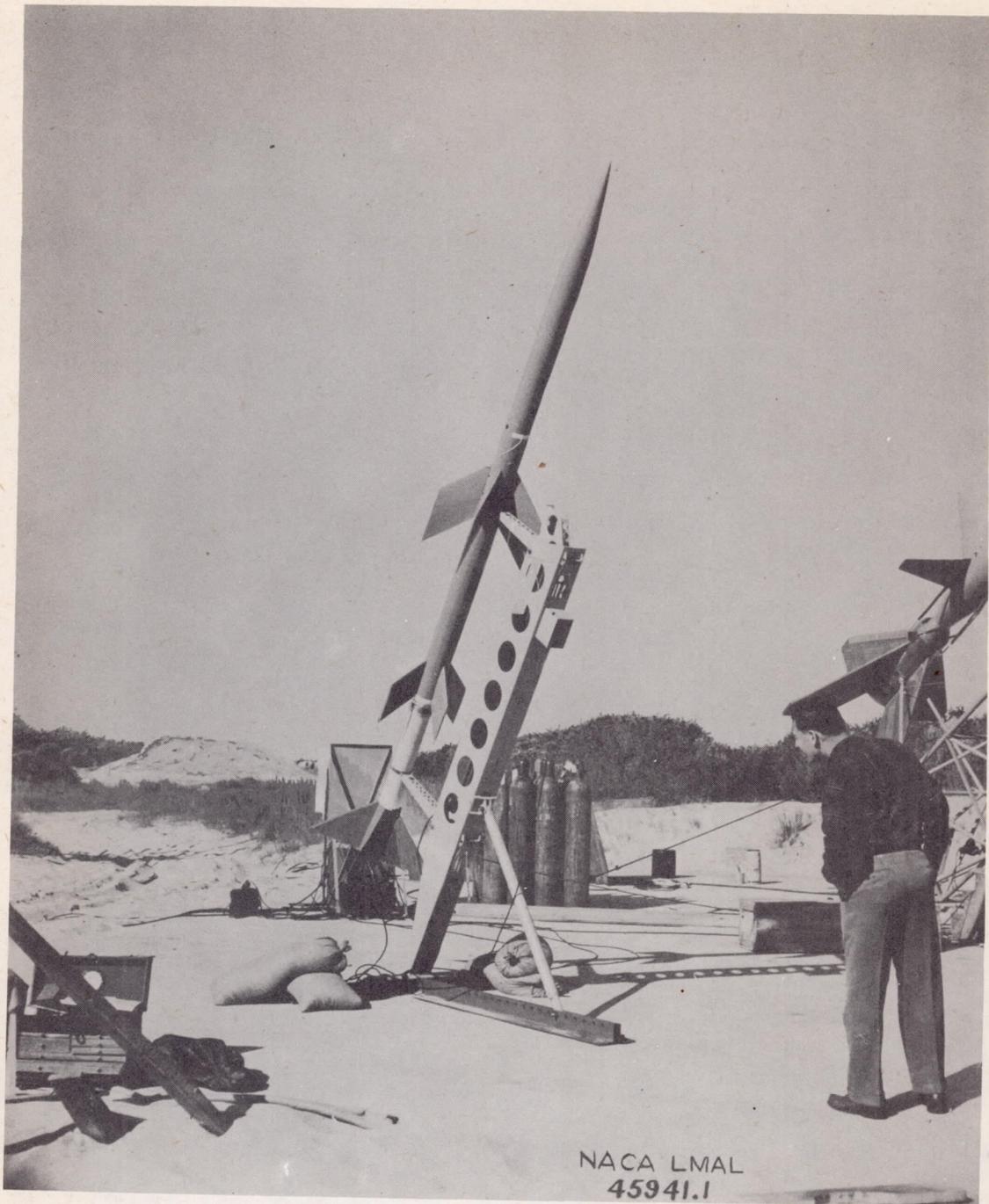
Figure 8.-   The RM-1 model with booster tail
mounted on launching rack.
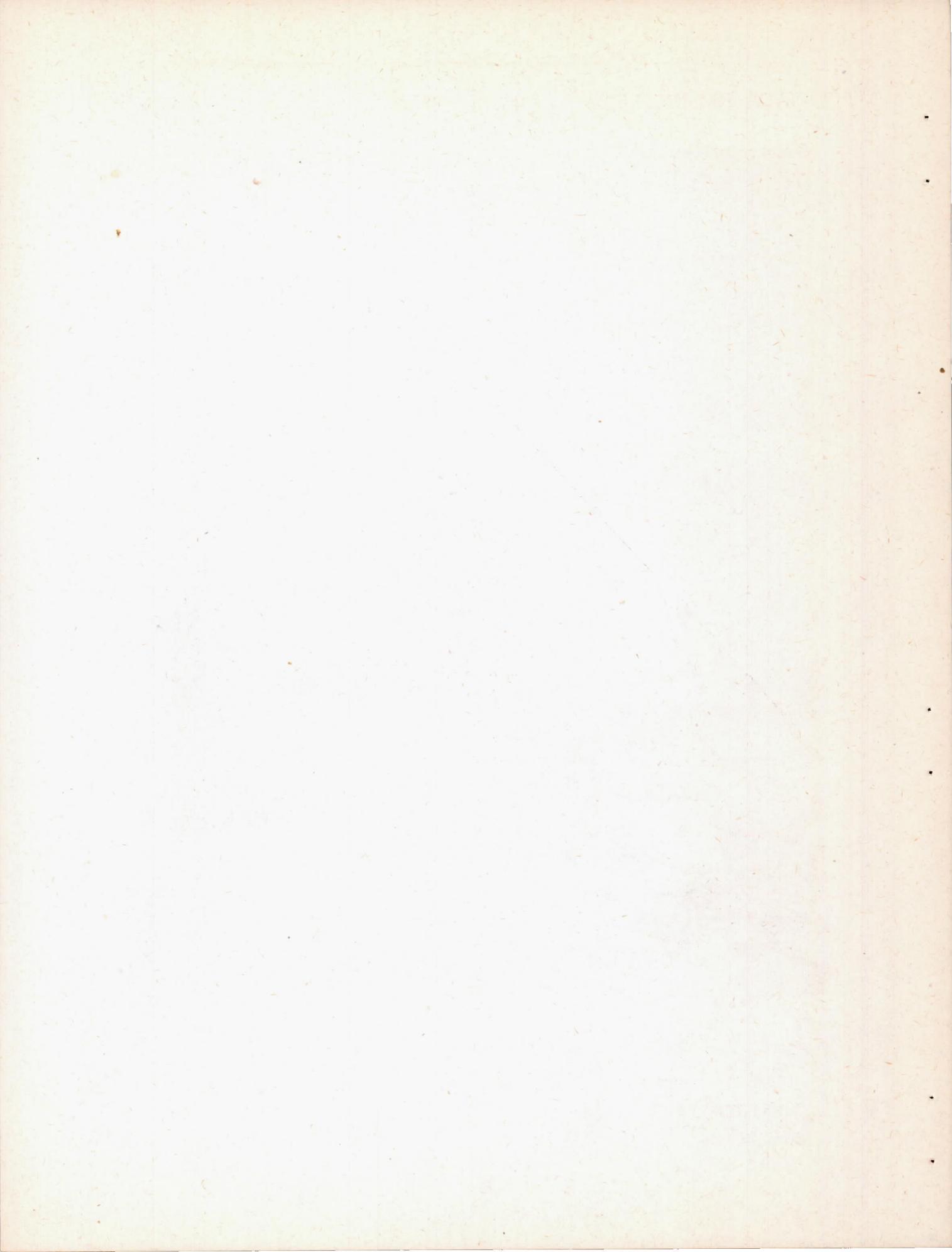
CONFIDENTIAL

Figure 9.-   Continuous-wave Doppler radar set (AN/TPS-5).
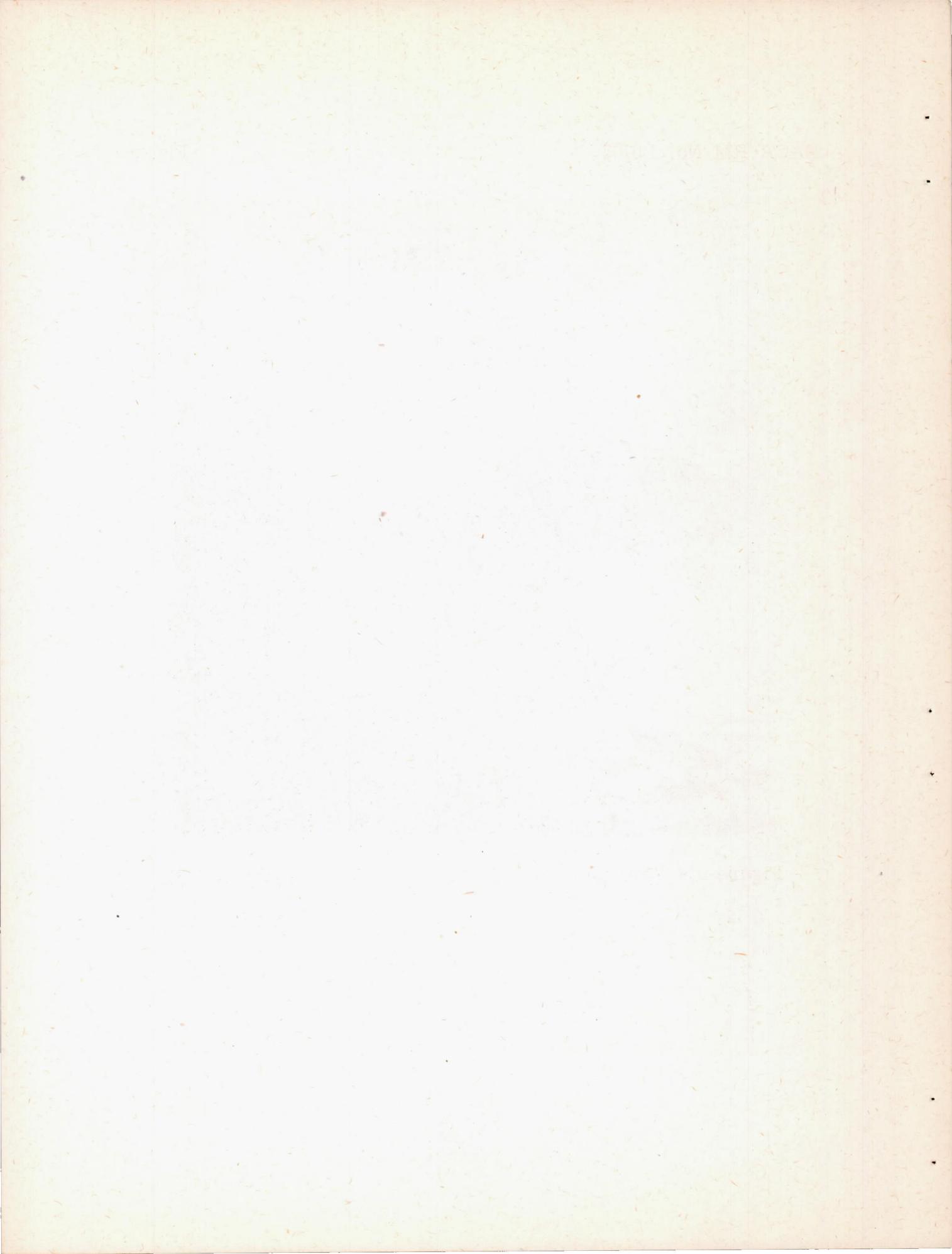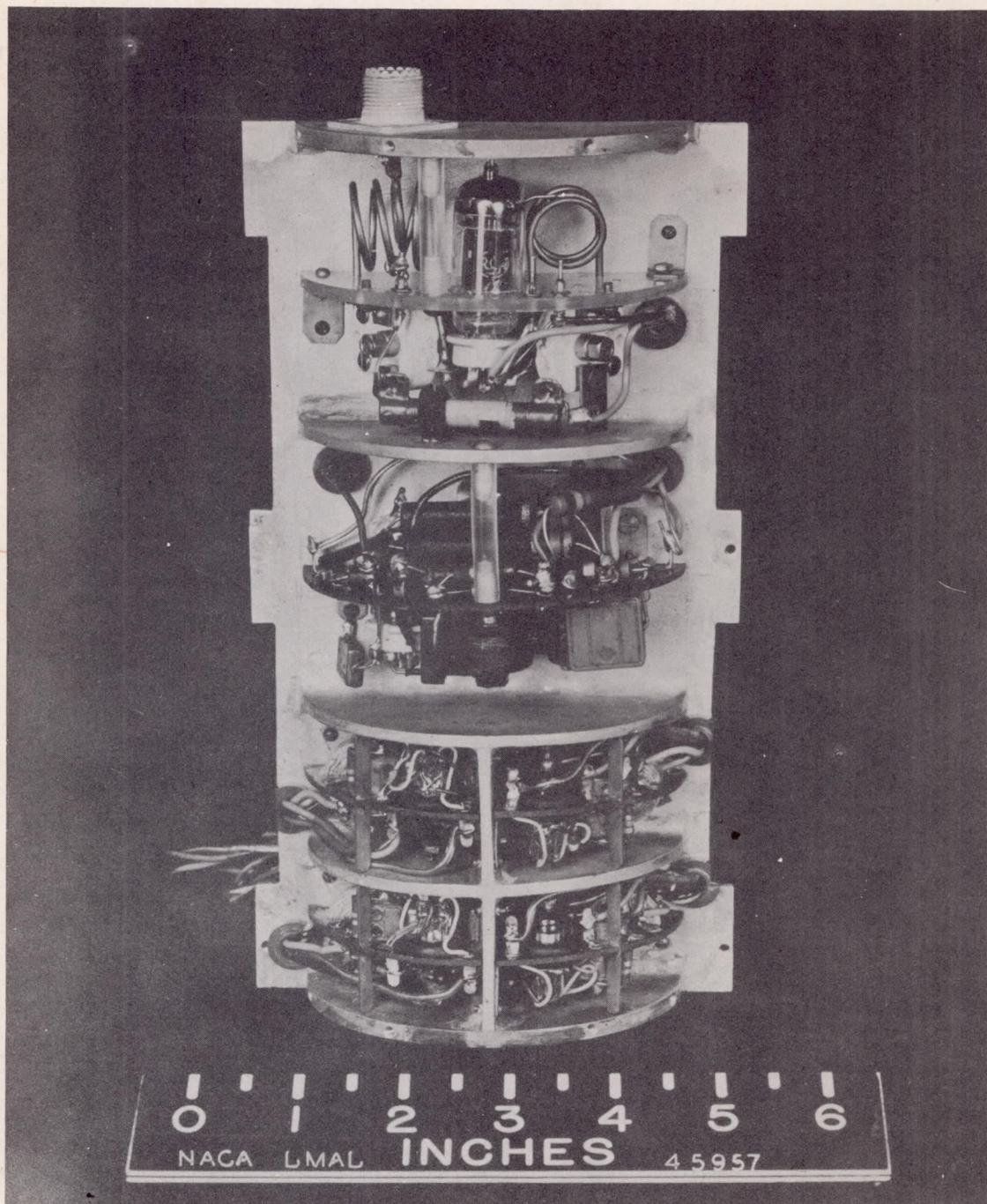
Figure 10.-   Radio-transmitter part of RM-1 model four-channel
telemeter.

CONFIDENTIAL
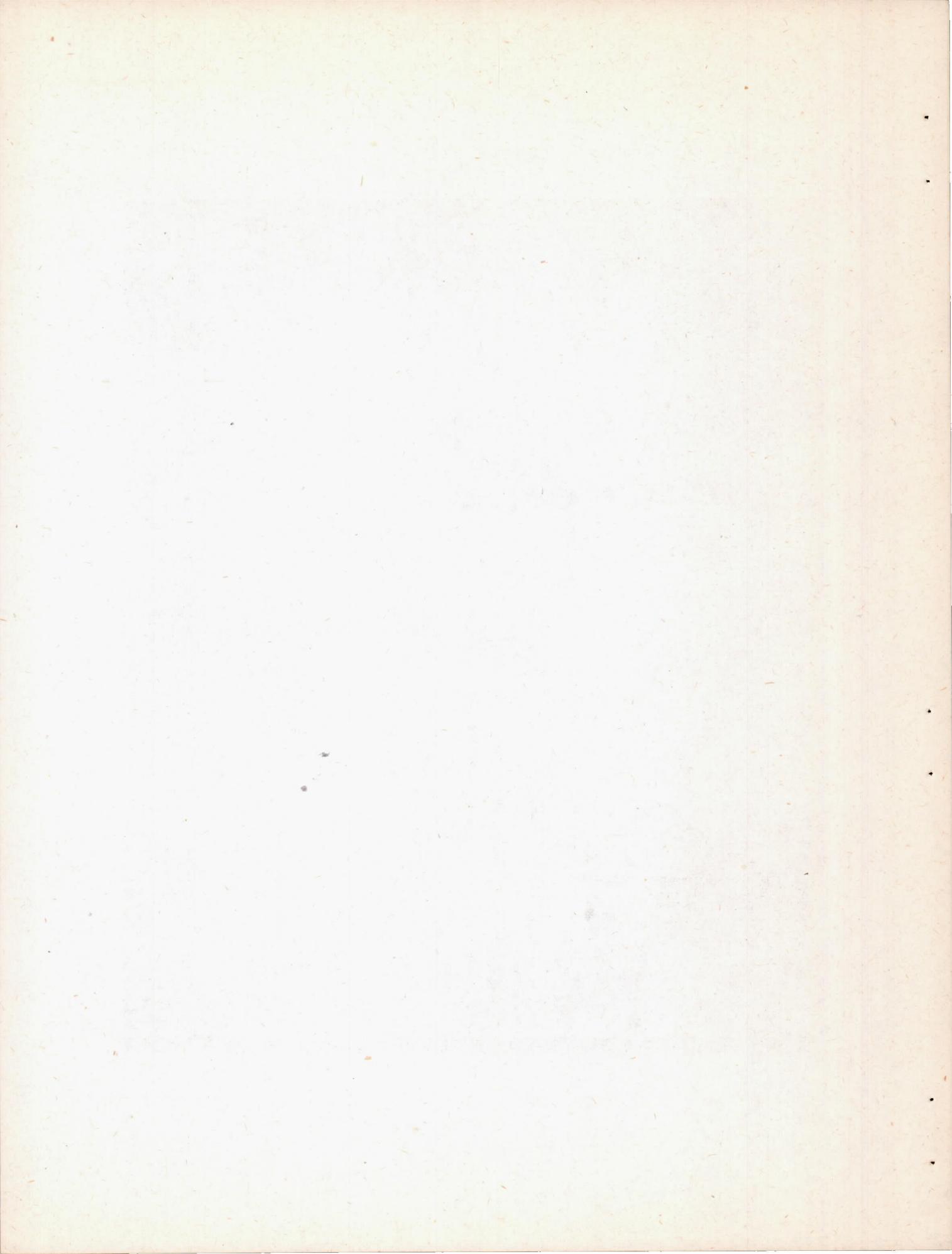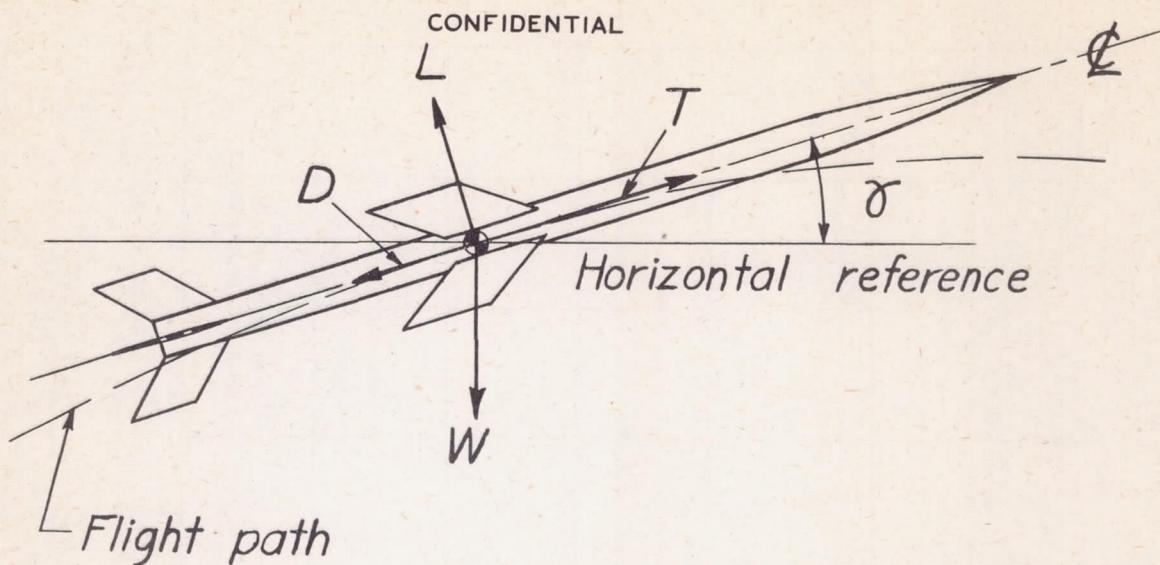
(a) External forces on airplane in free flight.
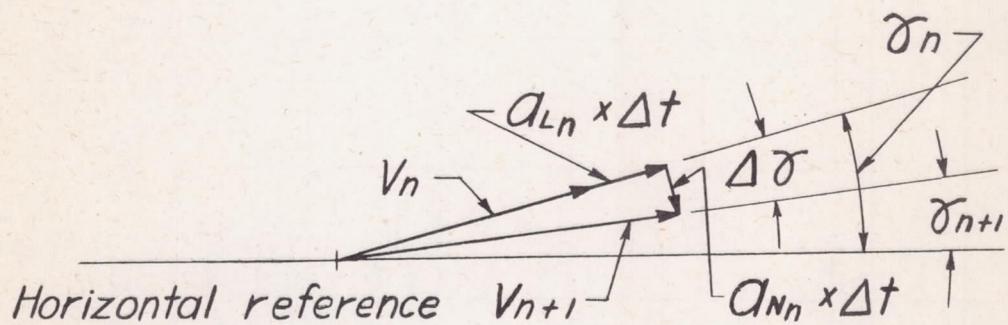
(b) Vectorial representation of iterant flight-
     path relationships (equation (8)).

CONFIDENTIAL

Figure 11.— RM-1 flight-path nomenclature.

Fig. 12
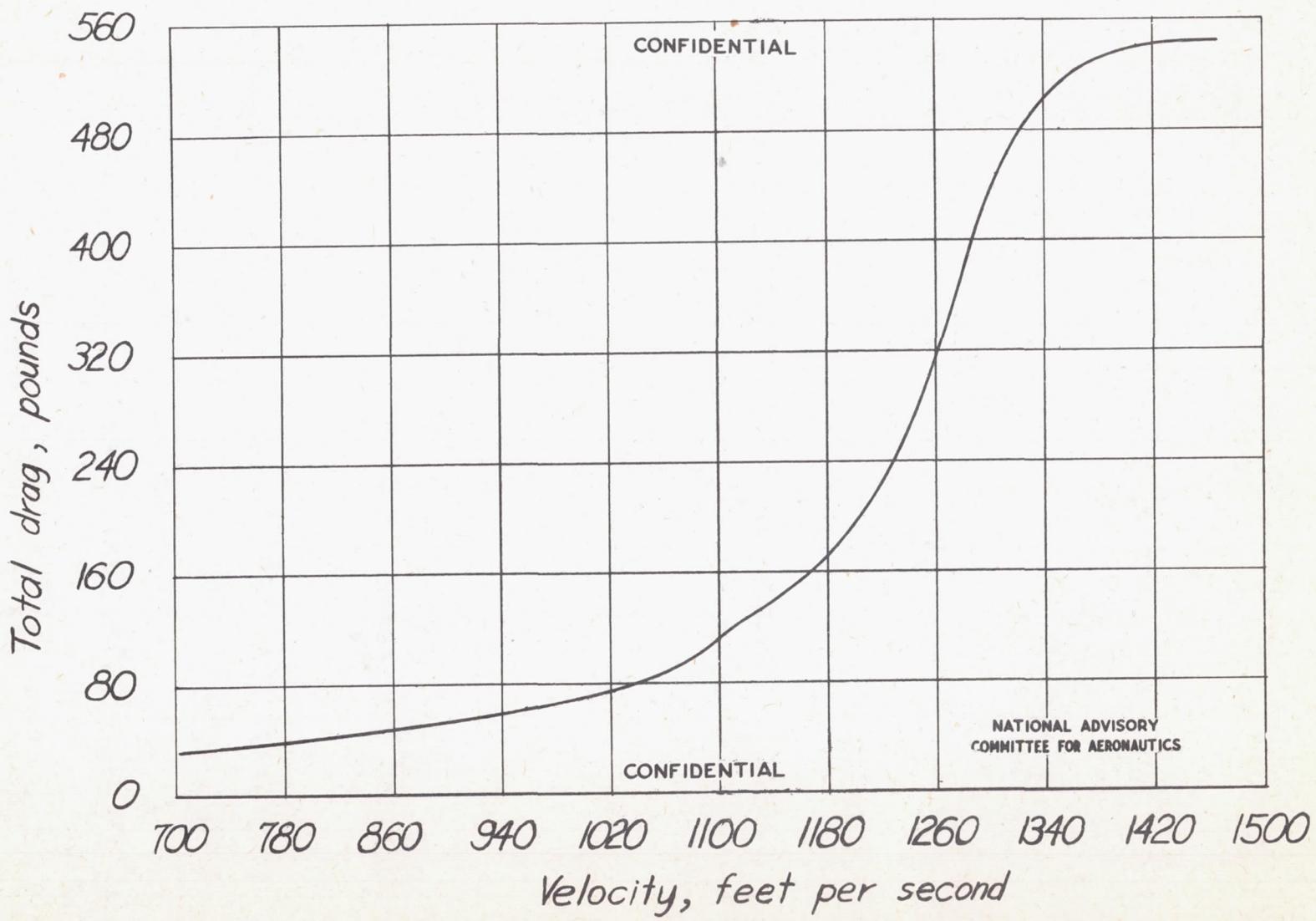
Figure 12.— Estimated drag curve for RM-1 configuration.
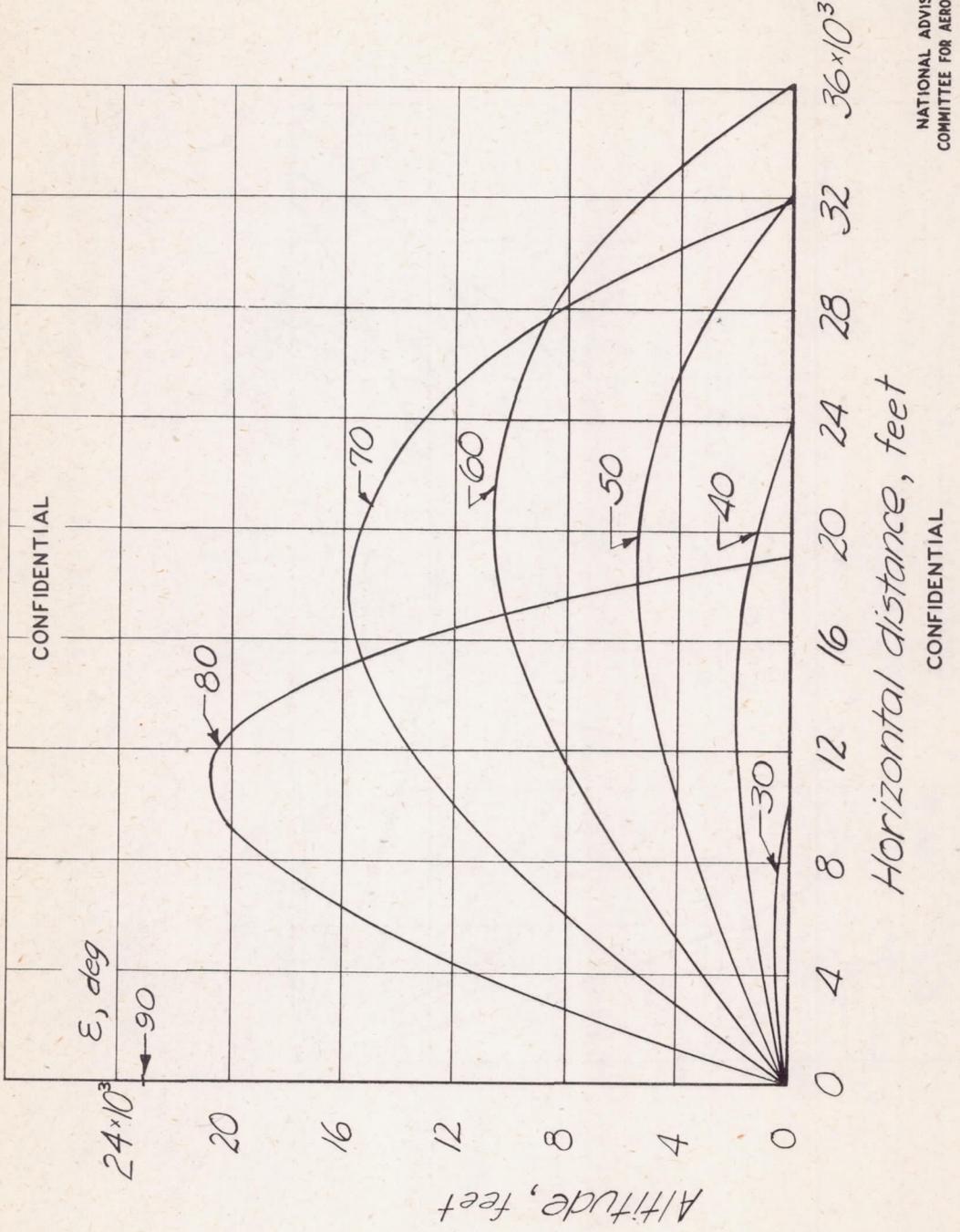
Figure 13.- Variation of zero-lift trajectory of RM-1 with launching angle. Booster-on condition.

Fig. 14   NACA RM No. L6J23
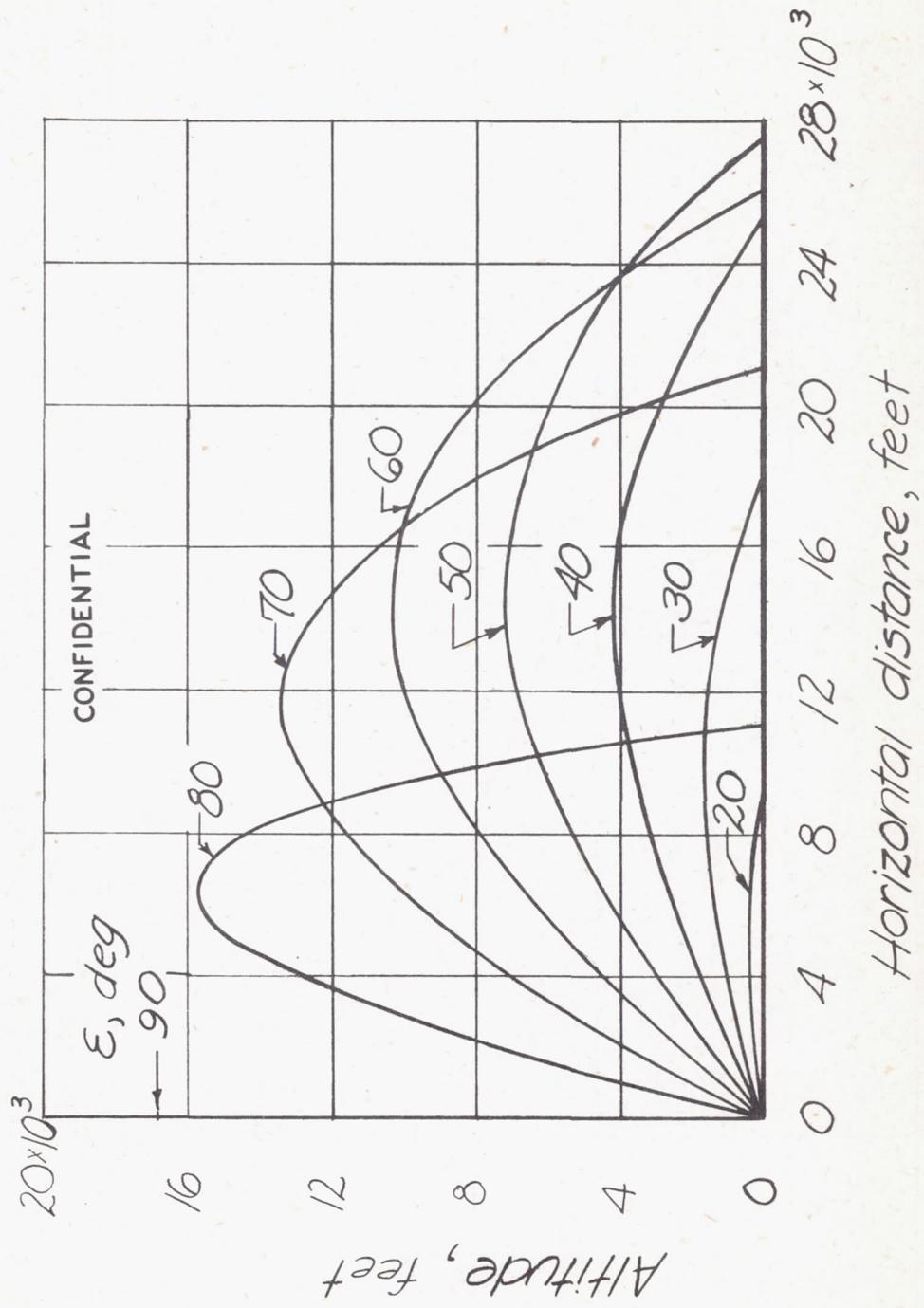
Figure 14.- Variation of zero-lift trajectory of RM-1 with launching angle. Booster-off condition.

CONFIDENTIAL

With booster

Without booster

CONFIDENTIAL

Maximum velocity, V, feet per second

Launching angle, ε, degrees

NATIONAL ADVISORY
COMMITTEE FOR AERONAUTICS
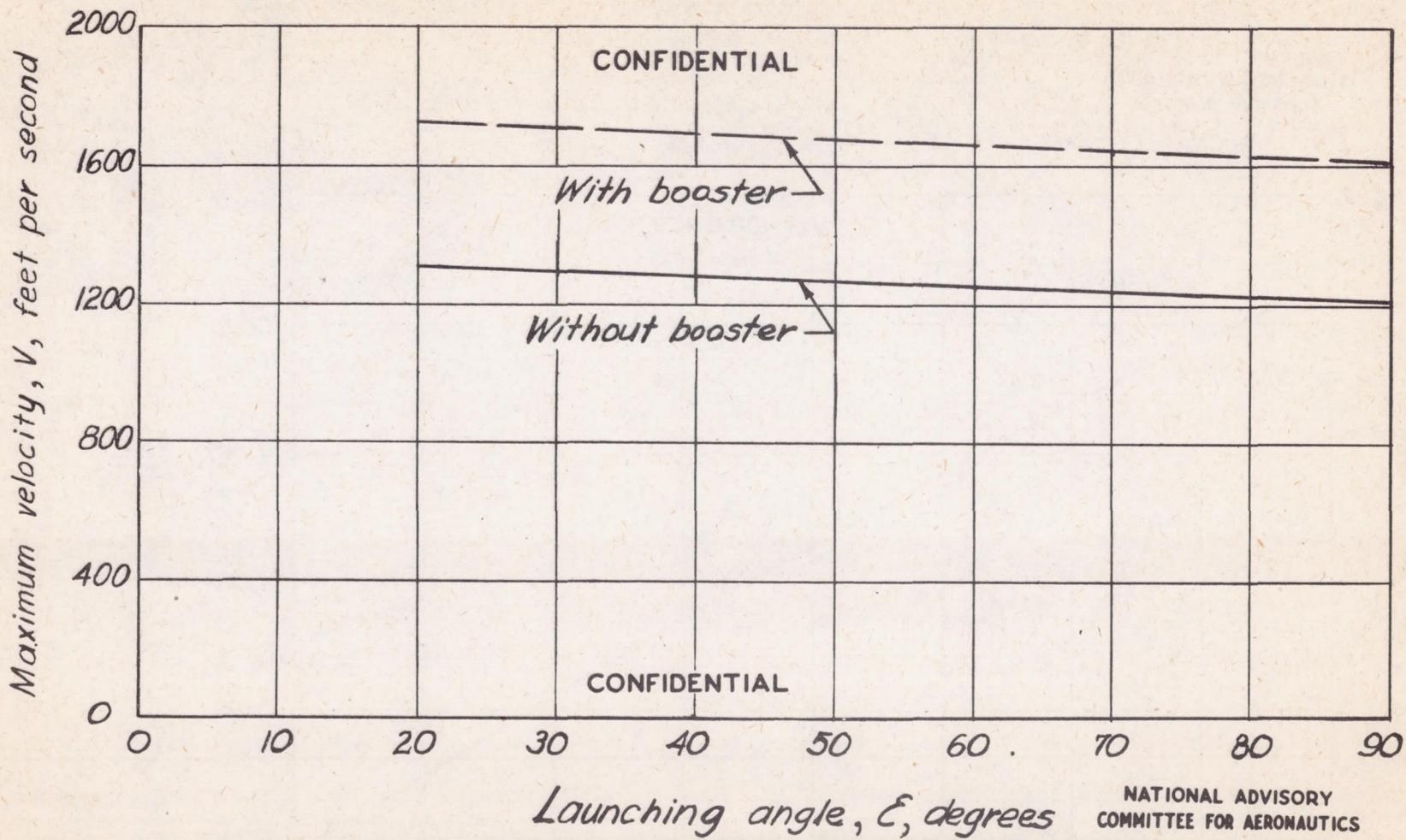
Figure 15.— Variation of calculated maximum speed with launching angle of an RM-1 configuration. Gross weight, 110 pounds; 65-pound booster.

Fig. 15

Fig. 16

CONFIDENTIAL

CONFIDENTIAL

NATIONAL ADVISORY
COMMITTEE FOR AERONAUTICS
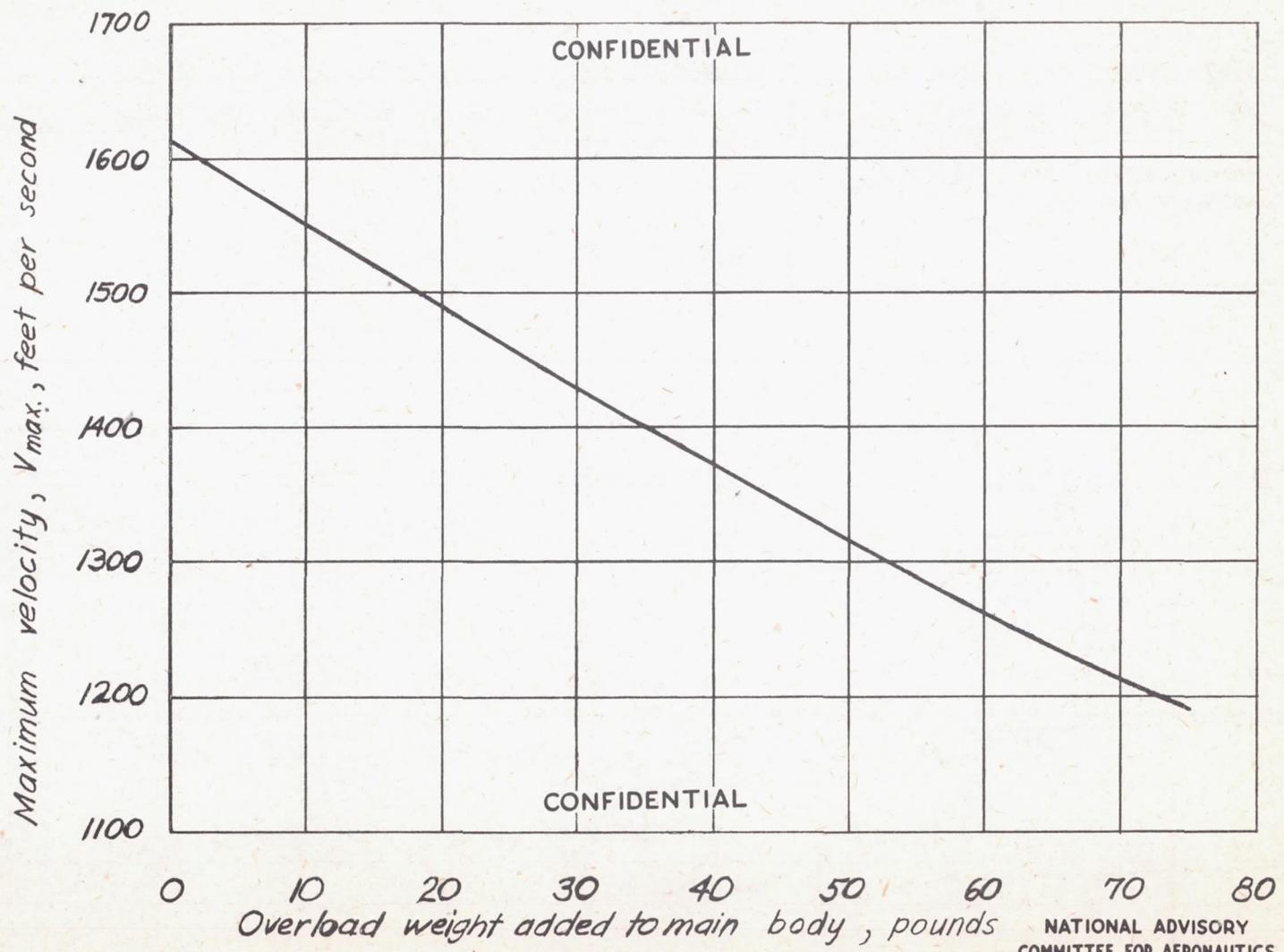
Figure 16.- Variation of calculated maximum velocity with overload weight for RM-1 configuration. Design weight, 110 pounds; 65-pound booster; $\varepsilon = 60°$.

Figure 17.-   Launching of RM-1 dummy with booster tail.   (First flight)
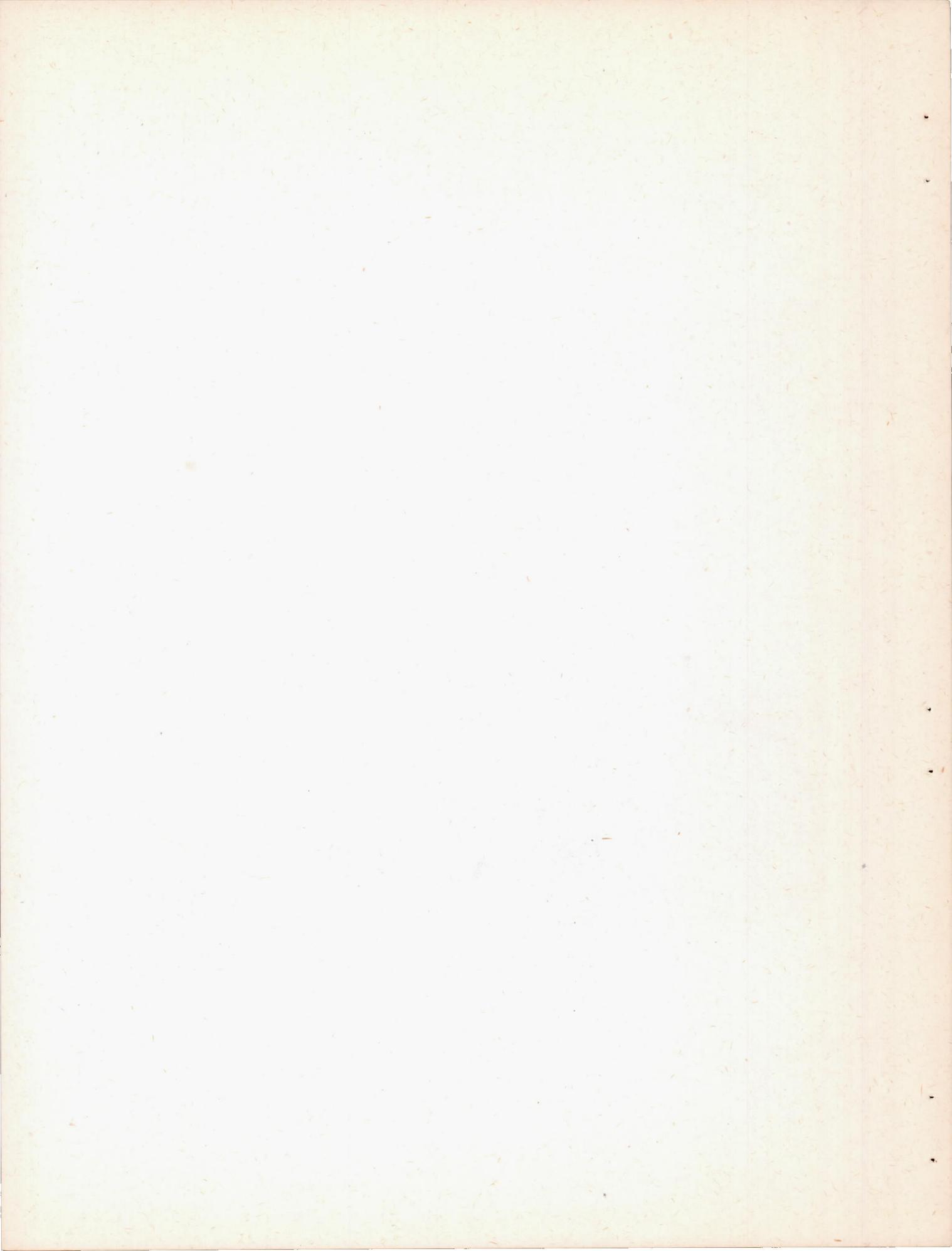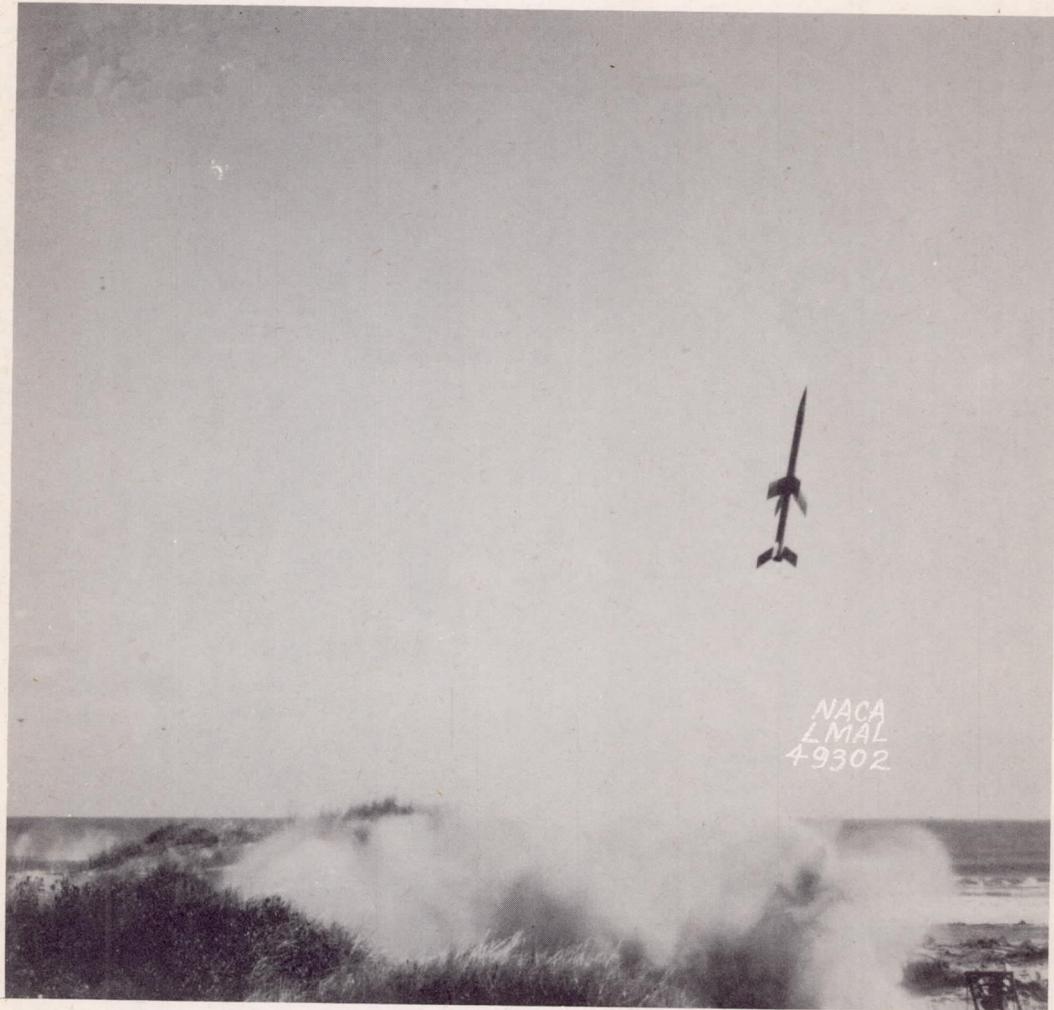
Figure 18.-   Launching of RM-1 dummy without booster
        tail.   (Second flight.)
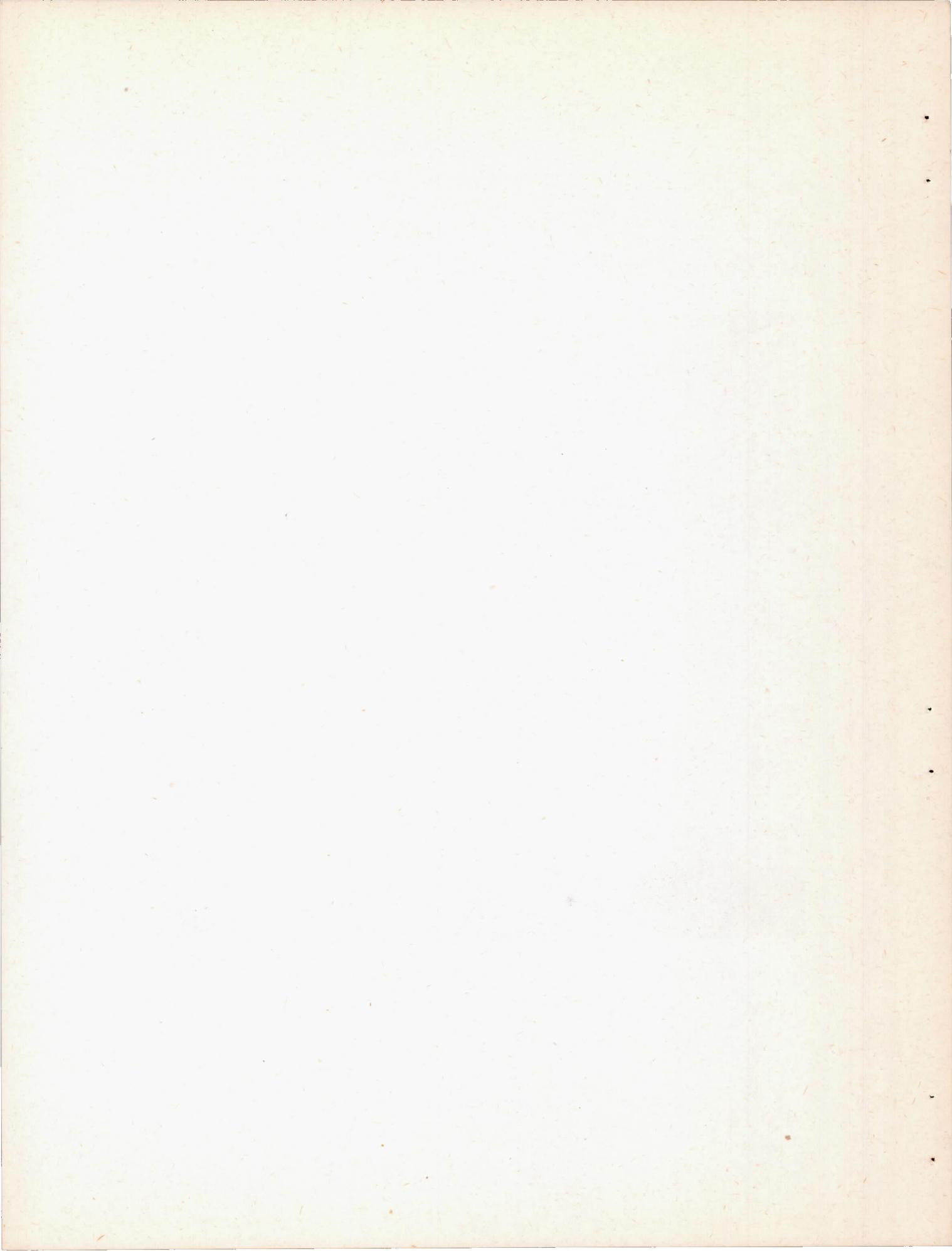
CONFIDENTIAL
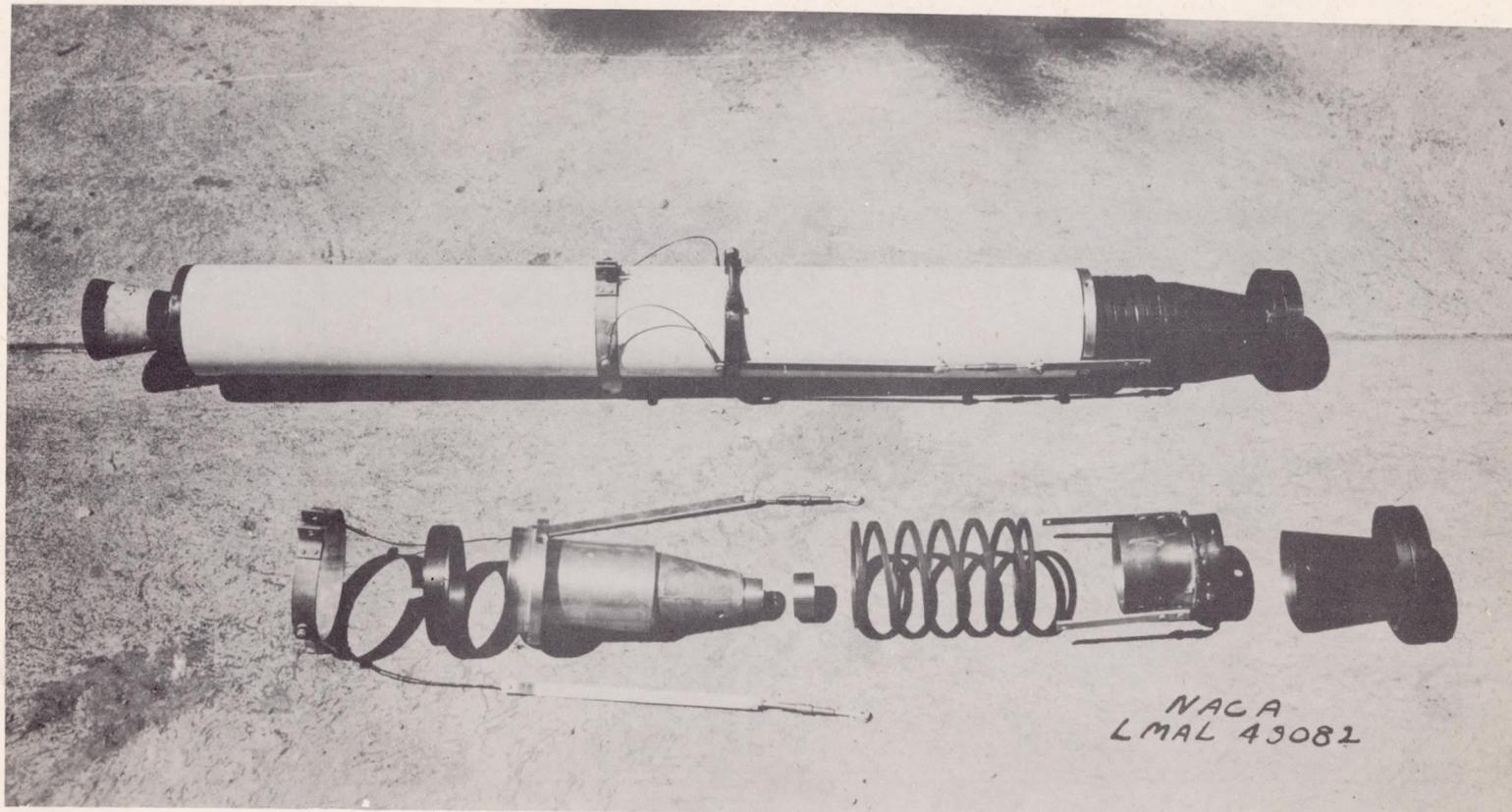
Figure 19.- Revised booster-rejection mechanism of RM-1 model.

CONFIDENTIAL

Fig. 19
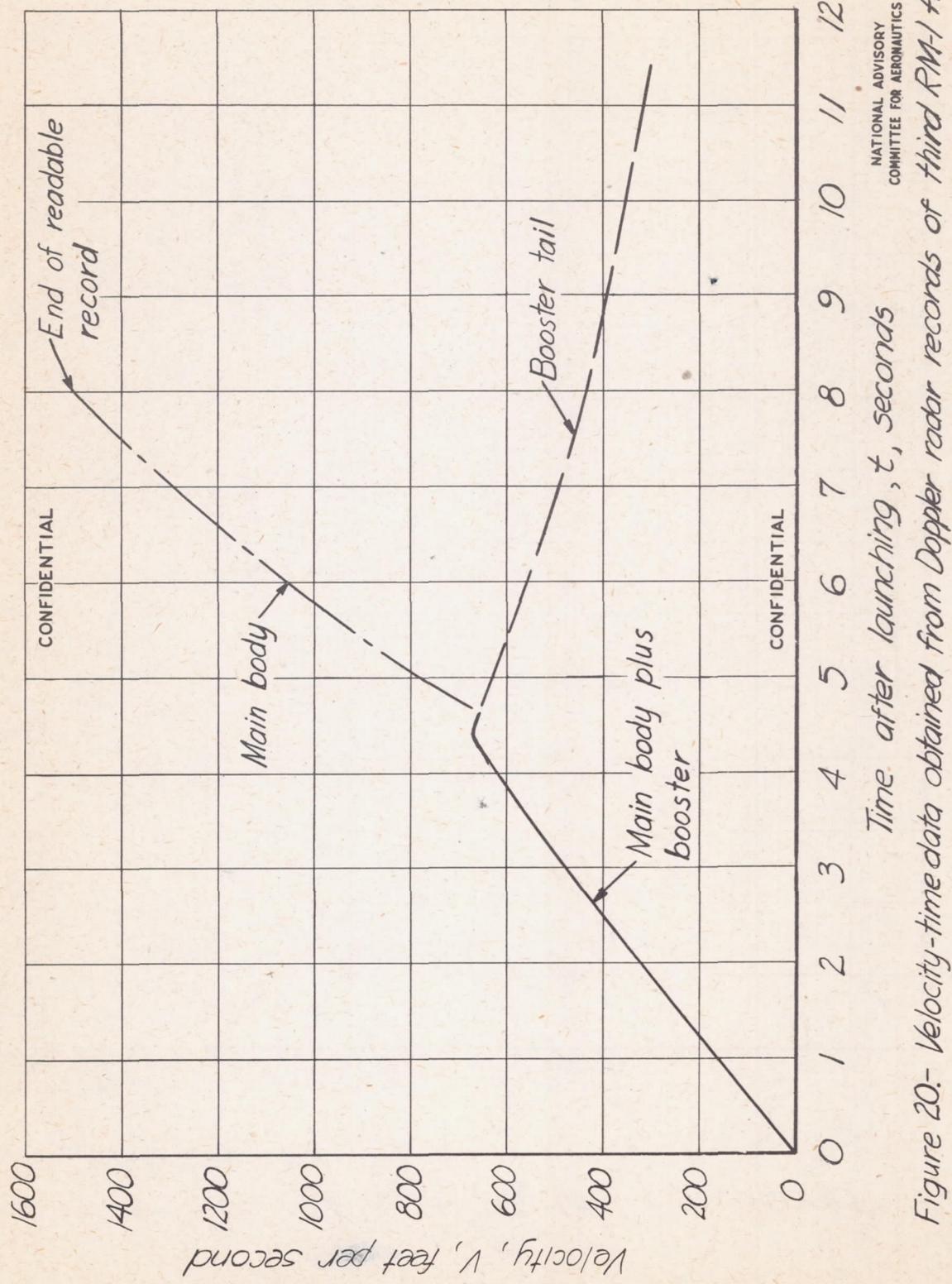
Figure 20.- Velocity-time data obtained from Doppler radar records of third RM-1 flight.

Fig. 21
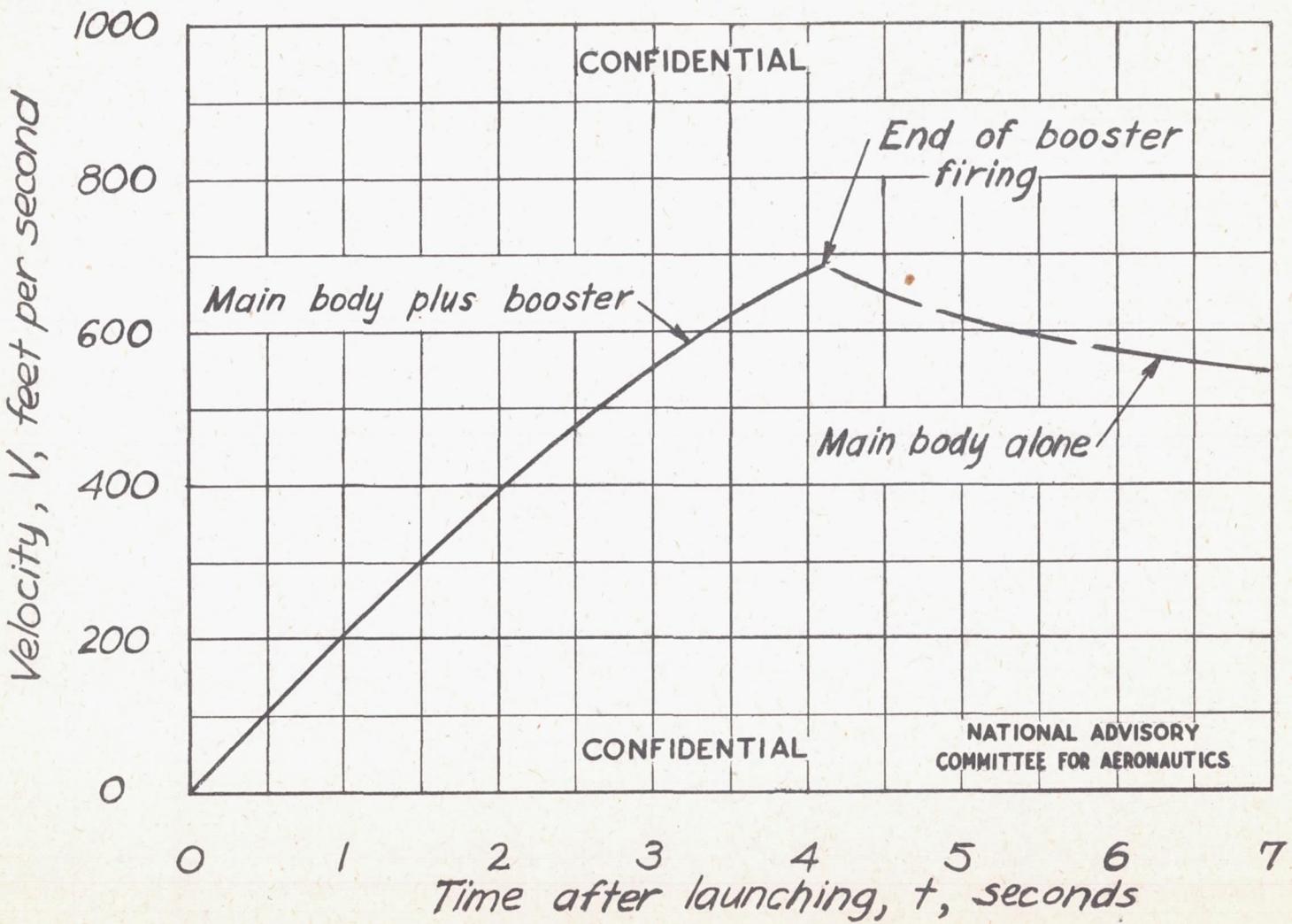
Figure 21.- Velocity-time record obtained by Doppler radar from fourth flight of RM-1 research model.
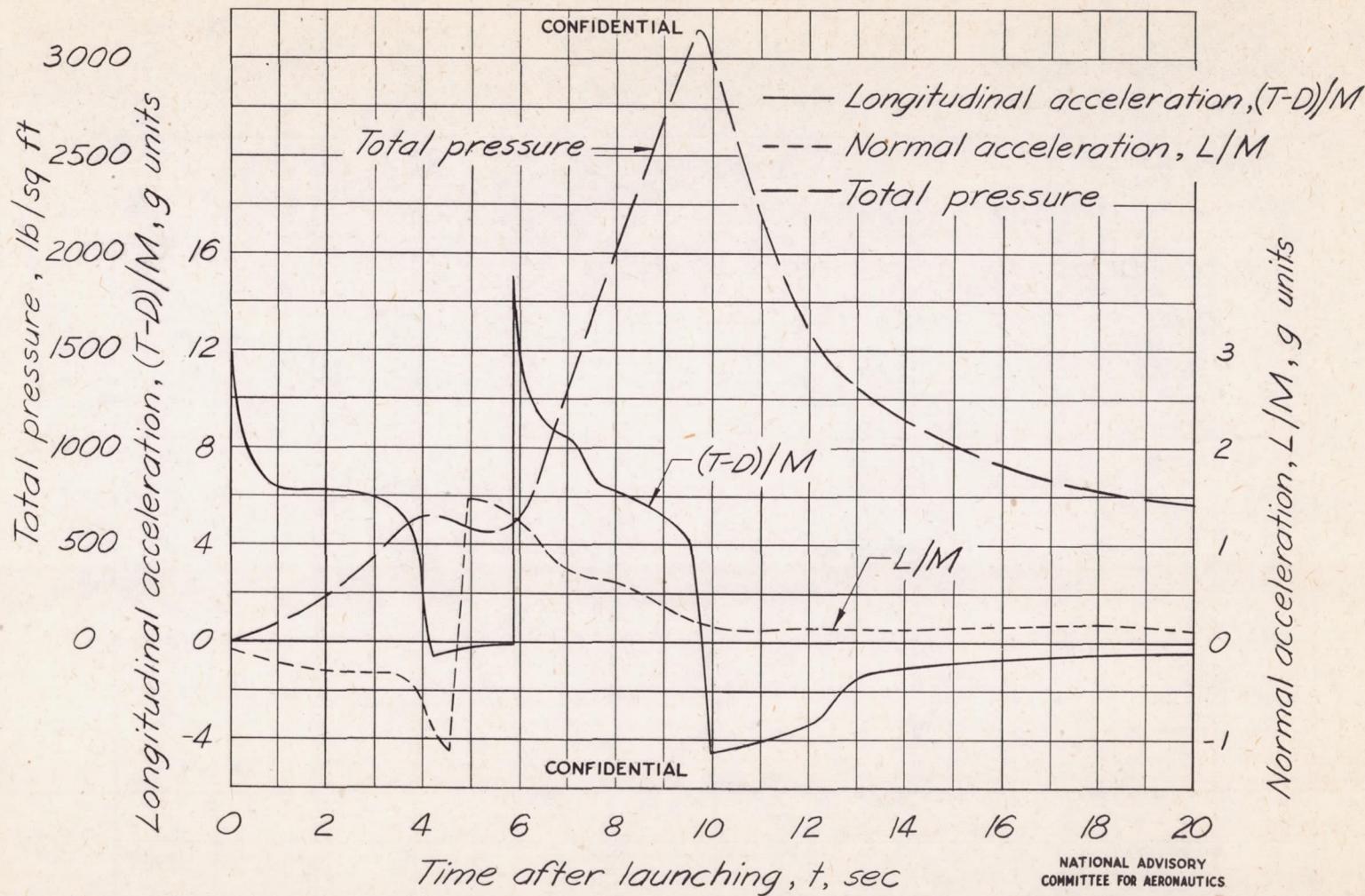
Figure 22.– Time histories of total pressure and normal and longitudinal accelerations obtained from telemetered data of fifth flight of RM-1 model.

Fig. 22

Fig. 23
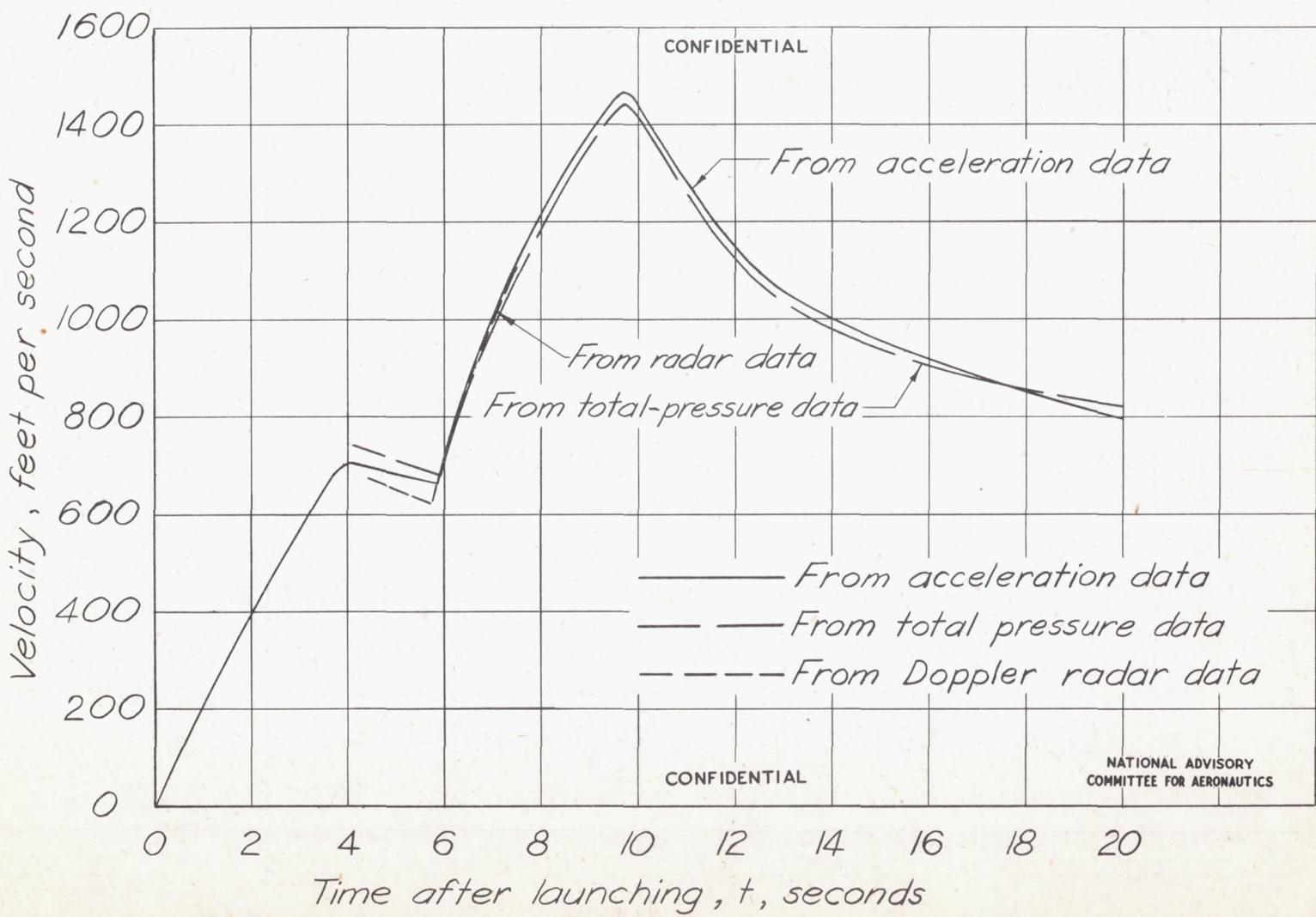
Figure 23. - Comparison of velocity measurements of the RM-1 configuration in flight.
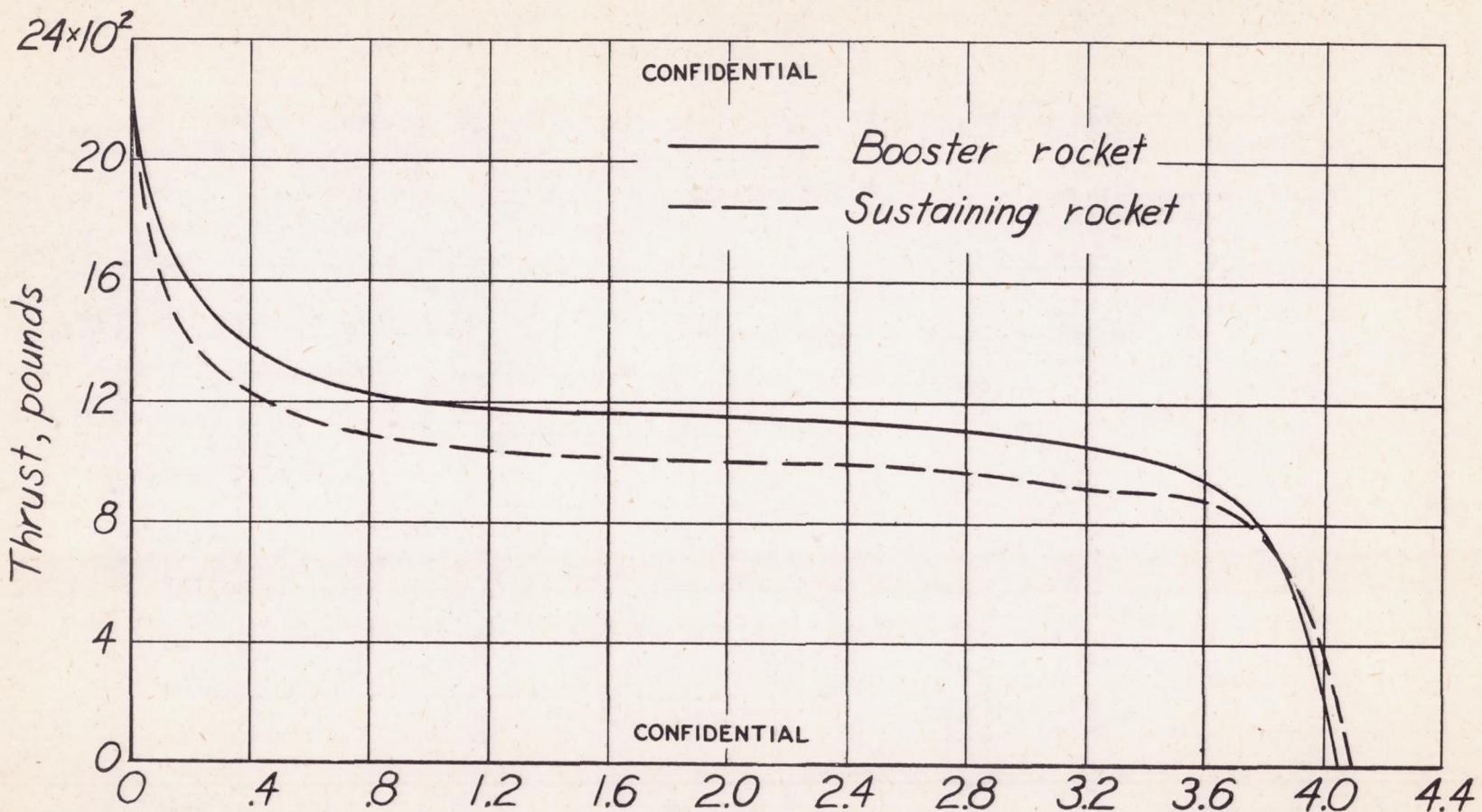
Figure 24. — RM-I rocket thrust-time curves.

Fig. 24

Fig. 25

Figure 25. - Drag characteristics of the RM-1 without booster.

CONFIDENTIAL

RM-1 , A =1.41 , Λ =45°

RM-2 , A = 1.04, Λ =45°

RM-2 , A =2.15, Λ =45°

Drag coefficient, C_D
(based on exposed wing and fin area)

.06

.05

.04

.03

.02

.01

0

CONFIDENTIAL

NATIONAL ADVISORY
COMMITTEE FOR AERONAUTICS

.6   .7   .8   .9   1.0   1.1   1.2   1.3   1.4

Mach number, M
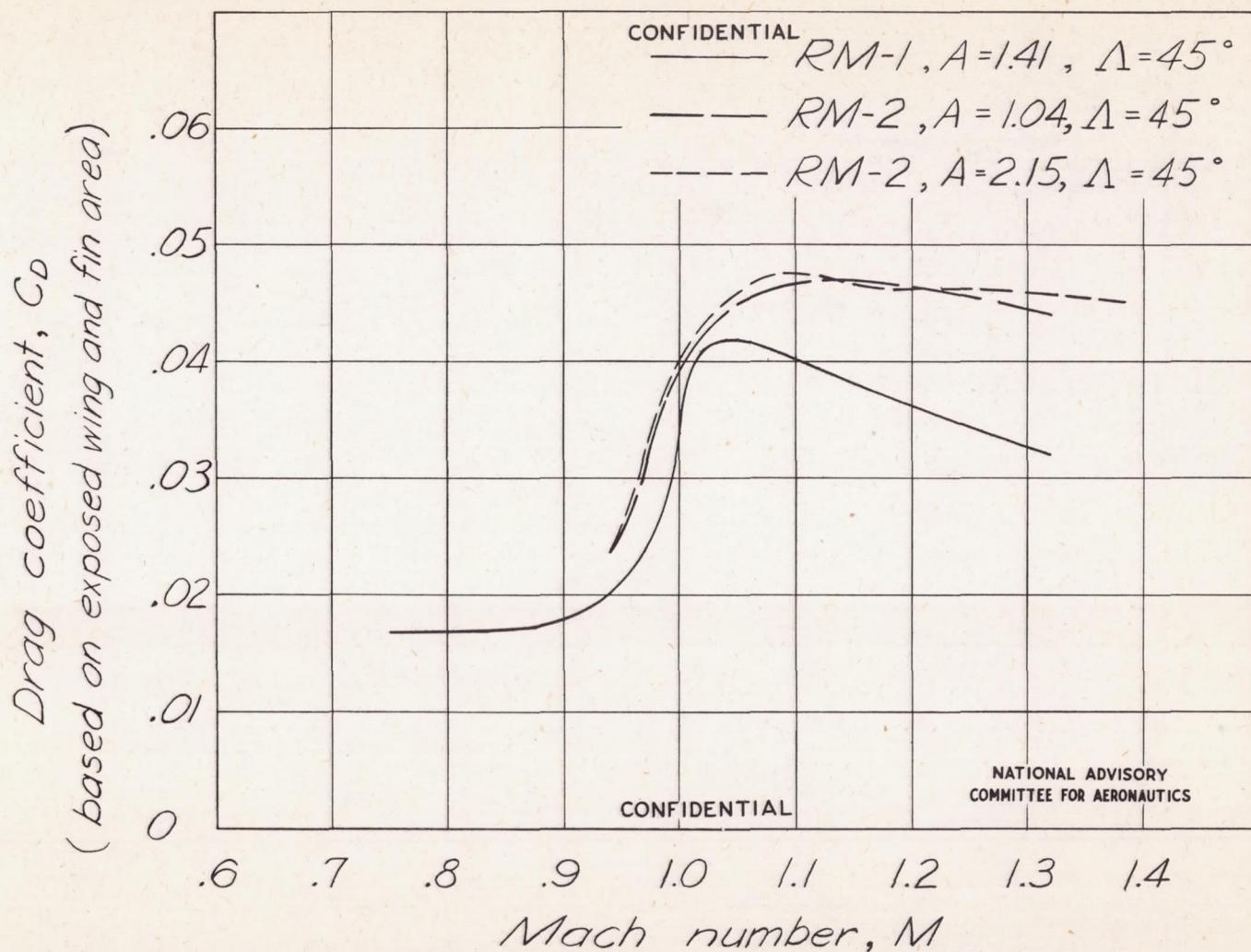
Figure 26.- Comparison of drag characteristics of the RM-1 model
with drag characteristics of the RM-2 configuration.

Fig. 26

Fig. 27
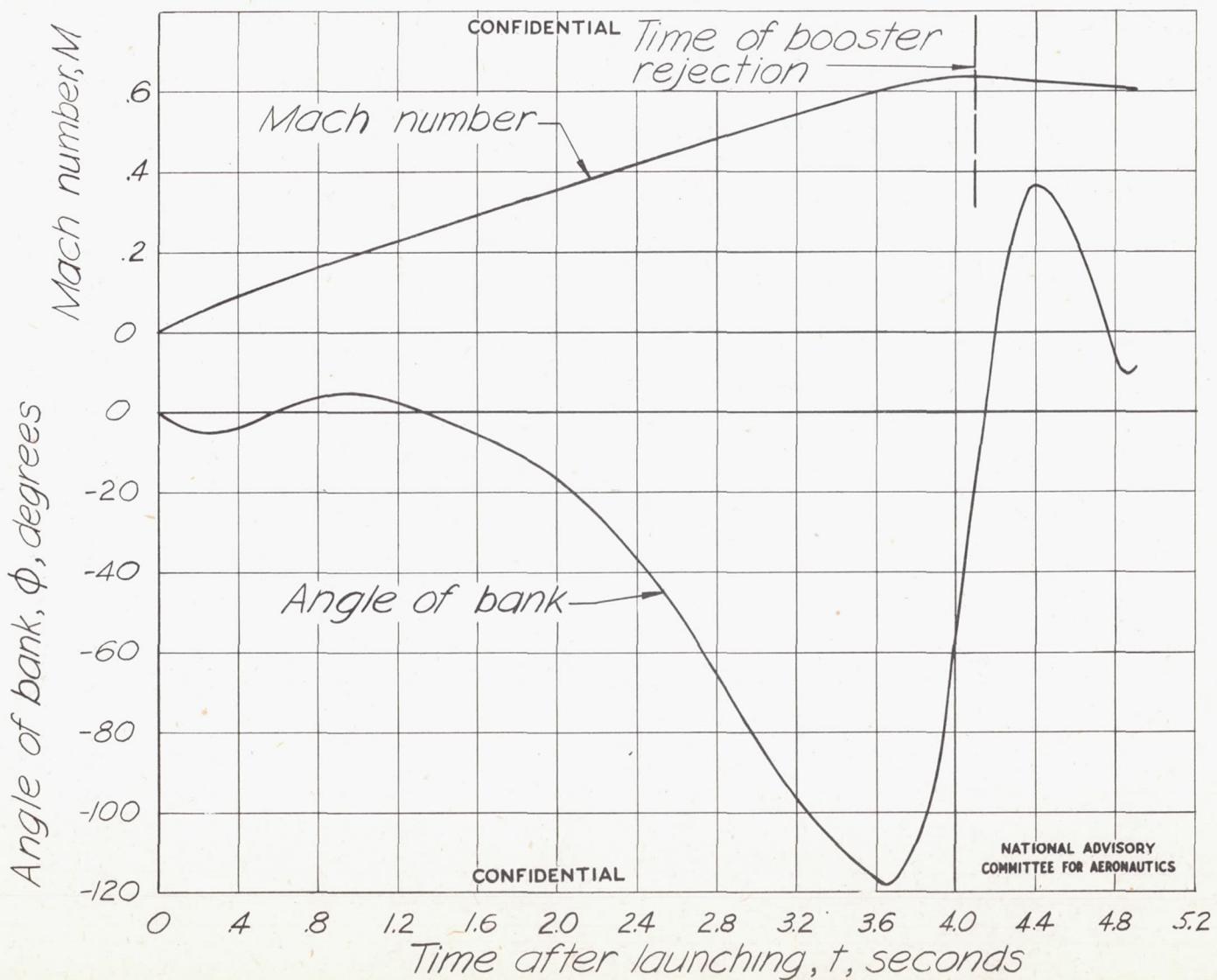
Figure 27.- Telemeter time history of roll characteristics of the RM-1 in flight.

Fig. 28
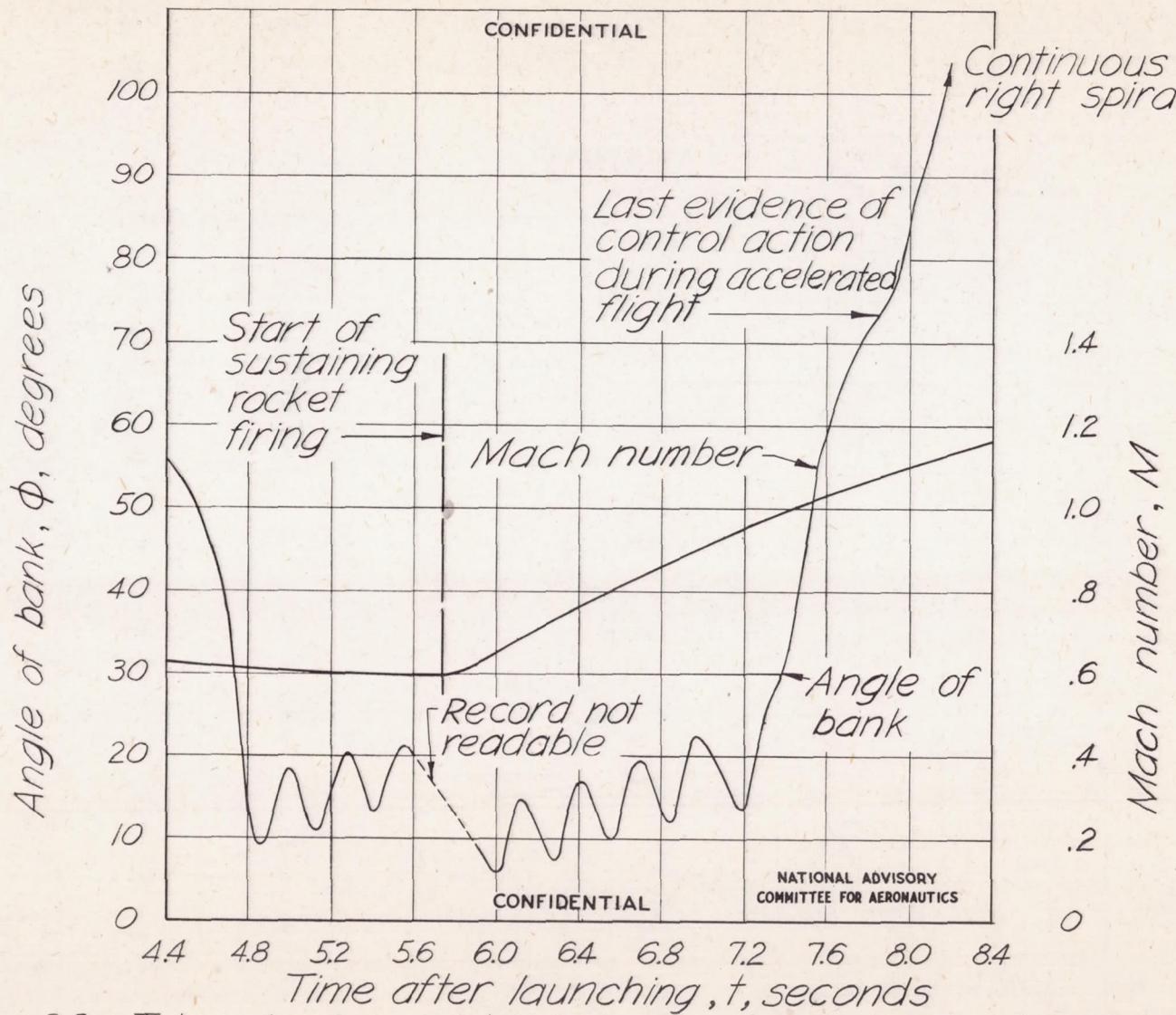
Figure 28. – Telemeter time history of roll characteristics of the RM-1 in flight.
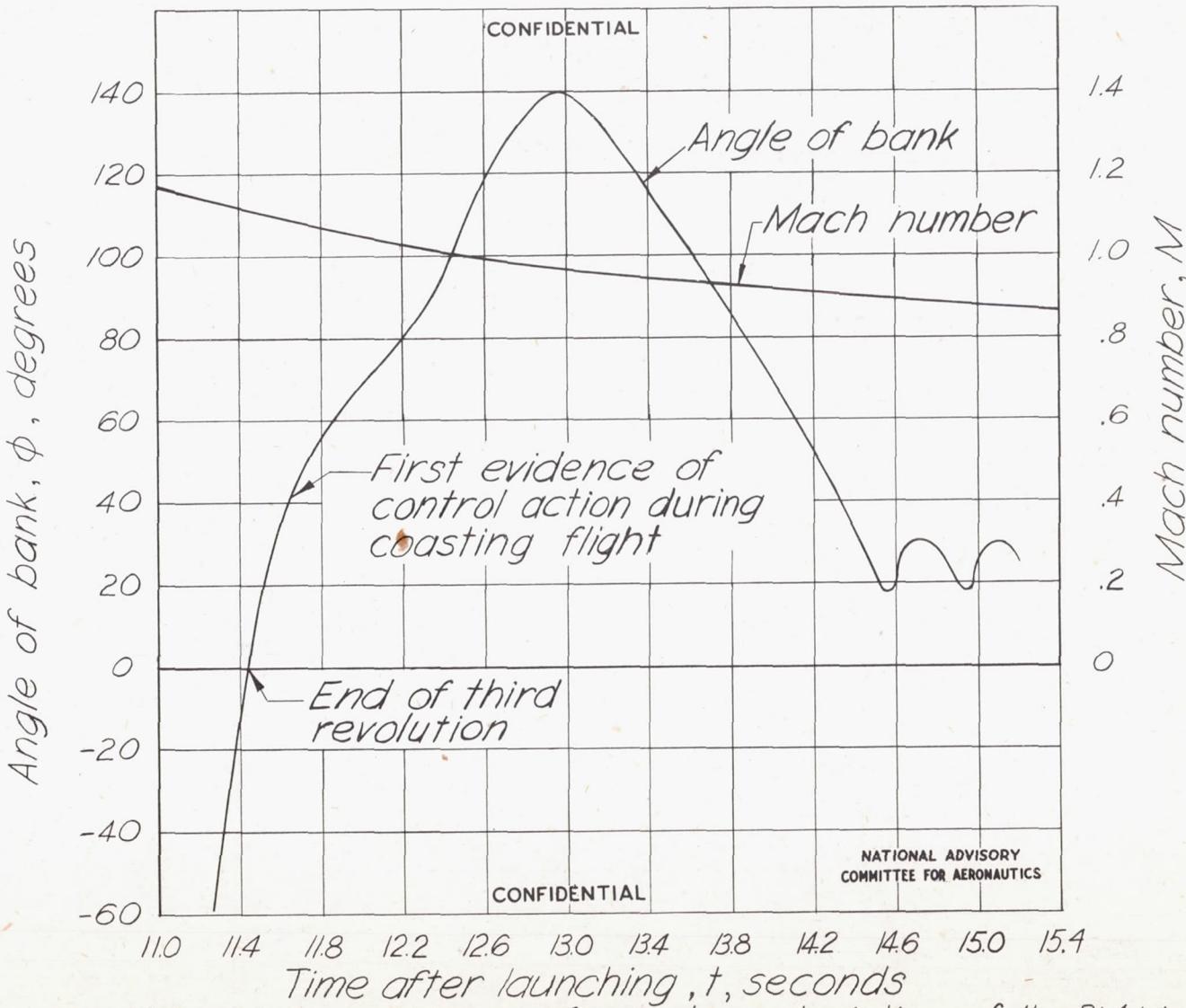
Fig. 29

Figure 29. - Telemeter time history of roll characteristics of the RM-1 in flight.

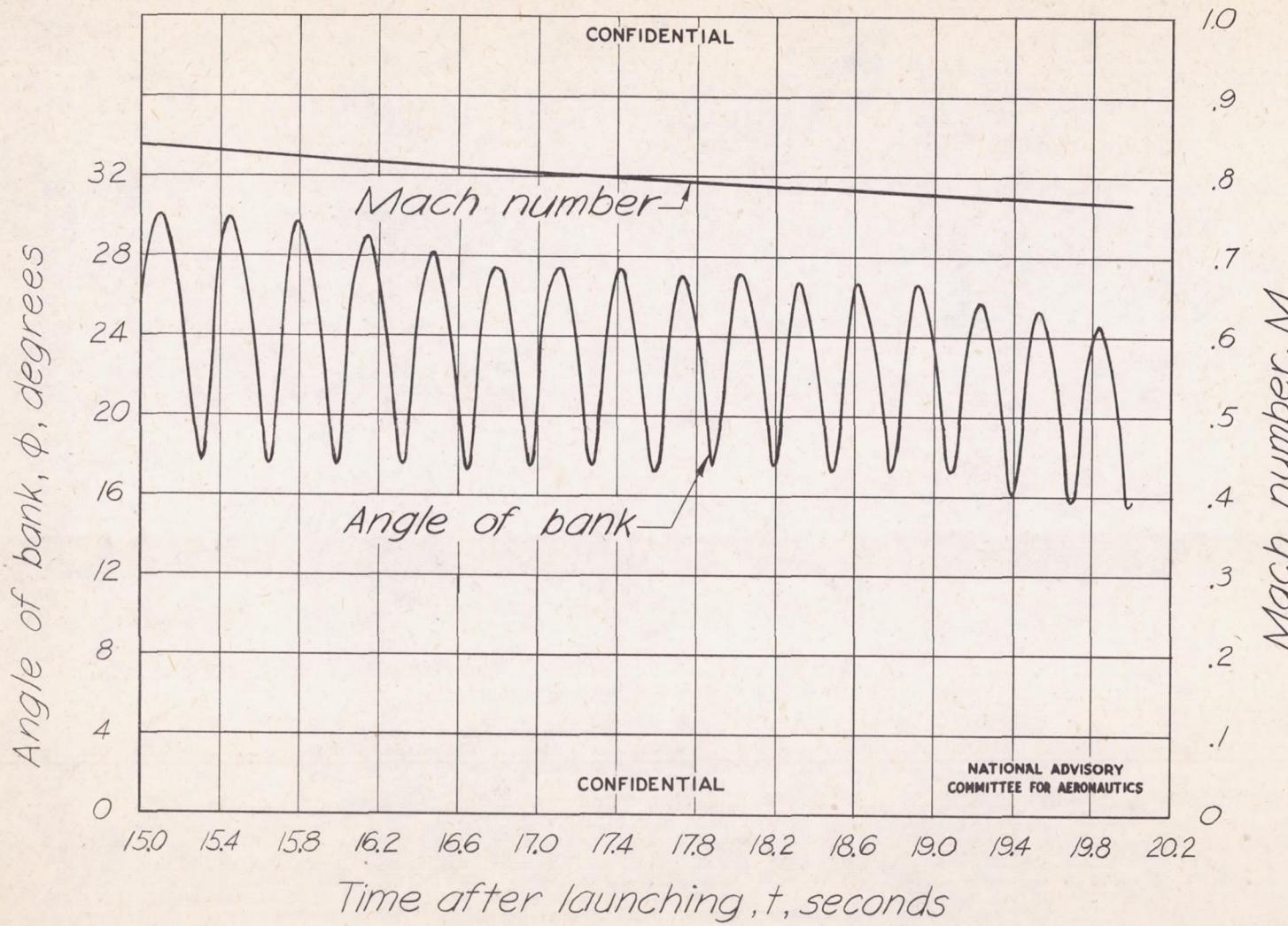Figure 30.–Telemeter time history of roll characteristics of the RM-1 in flight.
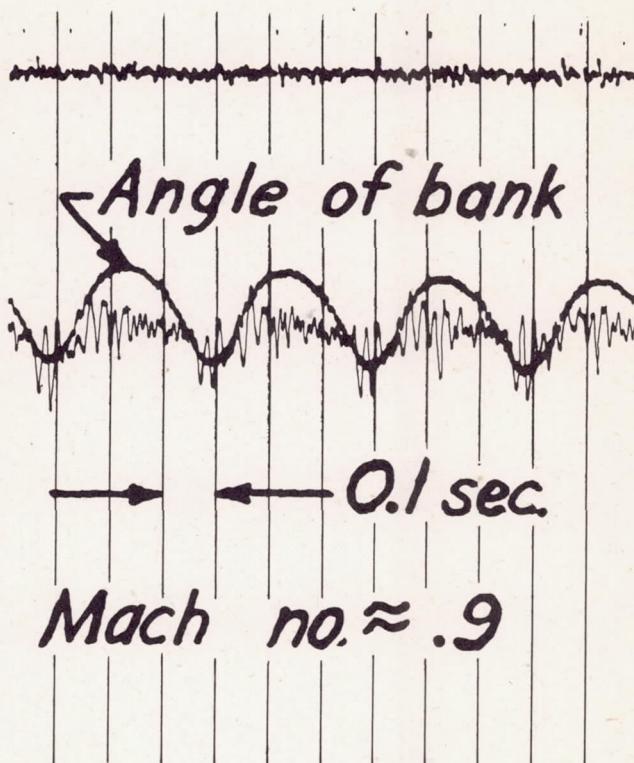
Fig. 30

Figure 31.- Telemeter record of roll oscillation of fifth flight of RM-1 model.

CONFIDENTIAL

**NATIONAL ADVISORY
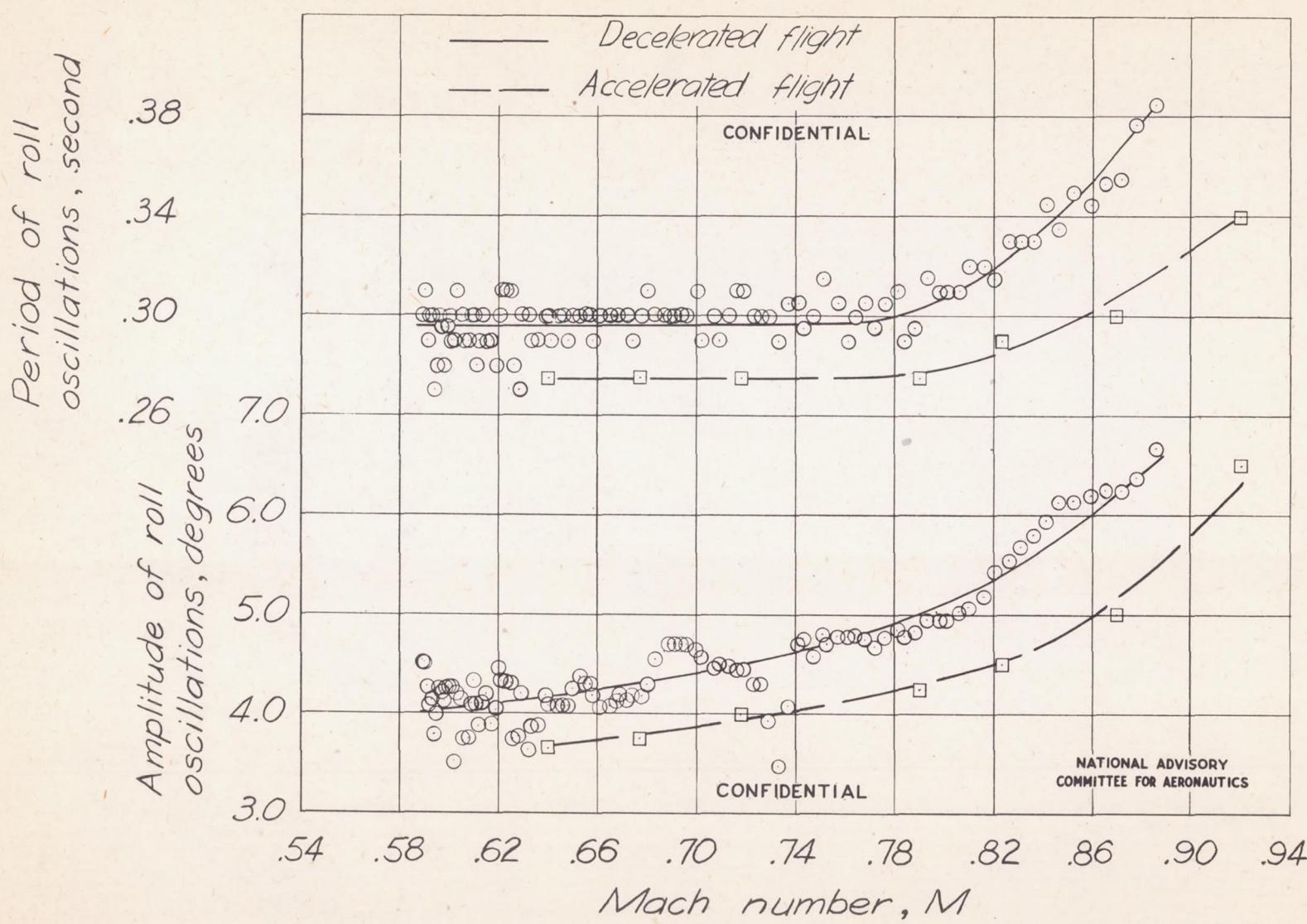COMMITTEE FOR AERONAUTICS.**

Figure 32.- Variation of characteristics of roll oscillation with Mach number.

Fig. 32